Journal of Hydrology 662 (2025) 133844

Contents lists available at ScienceDirect

Journal of Hydrology

journal homepage: www.elsevier.com/locate/jhydrol

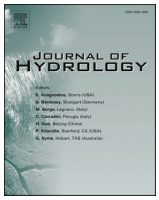

Research papers

Passive subsurface characterization in subsiding deltas: assessing land subsidence mitigation potential with frequency analyses of groundwater heads and superposing harmonic drivers

Felix Dörr [a,*], Jonas Bauer [a], Gabriel C. Rau [b], Remi Valois [c], Tran Viet Hoan [a,d], Van Cam Pham [a], Le Thi Mai Van [d], Anke Steinel [e], Franz Nestmann [f], Stefan Norra [g]

[a] Karlsruhe Institute of Technology (KIT), Institute of Applied Geosciences, Kaiserstraße 12, 76131 Karlsruhe, Germany
[b] School of Environmental and Life Sciences, The University of Newcastle, Callaghan, Australia
[c] Avignon University, INRAE, UMR 1114 EMMAH, F-84000 Avignon, France
[d] National Center for Water Resources Planning and Investigation (NAWAPI), No. 93, Lane 95, Vu Xuan Thieu Street, Sai Dong Ward, Long Bien District, Hanoi 100000, Viet Nam
[e] Federal Institute for Geosciences and Natural Resources (BGR), Stilleweg 2, D-30655 Hannover, Germany
[f] Karlsruhe Institute of Technology (KIT), Institute of Water and River Basin Management, Kaiserstraße 12, 76131 Karlsruhe, Germany
[g] Potsdam University, Institute of Environmental Sciences and Geography, Soil Sciences and Geoecology, Campus Golm, Building 12, 14476 Potsdam Golm, Germany

ARTICLE INFO

This manuscript was handled by D. Han, Editor-in-Chief, with the assistance of Xiaolong Geng, Associate Editor

Keywords:
Mekong Delta
Ca Mau
Earth and ocean tides
Tidal subsurface analysis

ABSTRACT

Many of the world's low-lying river deltas are experiencing severe land subsidence, posing significant challenges to sustainable development. Effective mitigation strategies require a thorough understanding of subsurface processes and comprehensive parameterization, which are often hindered by limited investigations and resources. In this context, passive subsurface characterization (PSC) methods are particularly advantageous, as they utilize existing datasets to estimate hydraulic and geomechanical properties of the subsurface. This study conducts a detailed frequency analysis of 43 groundwater head time series in the southern Vietnamese Mekong Delta, revealing harmonic signals and imprints of mechanical loading in groundwater heads. These signals are identified as a superposition of five key drivers: (i) Earth tides, (ii) atmospheric tides, (iii) ocean tides, (iv) river tides, and (v) anthropogenic groundwater extraction. By disentangling Earth and ocean tides from atmospheric tides at the semi-diurnal frequency S_2, the specific storage and elastic formation compressibility of the intensely exploited middle Pliocene aquifer are estimated to 5.9–7.8 · 10^{-6} m^{-1} and 6.4–7.5 · 10^{-10} Pa^{-1}, respectively. This indicates a low land rebound and water storage potential and therefore an insignificant subsidence mitigation potential of this confined aquifer. By revealing that groundwater pumping may leak into amplitude spectra and corrupt quantitative PSC, this study underscores that accurate parameter estimations require a careful disentanglement of various superposing drivers. While the complex interplay of multiple tidal forcings limited previous PSC-applications in subsiding deltas, the novel integration of ocean tide loading on the solid Earth enables PSC-parameter estimations in coastal groundwater systems.

1. Introduction

Land subsidence is a geohazard of global scale and relevance, with nearly two billion people living in affected areas (Davydzenka et al., 2024). Groundwater over-exploitation has been identified as one of the main causes for intensive large-scale land subsidence (Motagh et al., 2008; Sun et al., 1999; Poland and Davis, 1969). Coastal plains and river deltas are particularly vulnerable to subsidence-induced land loss due to

Abbreviations: BE, barometric efficiency; FFT, fast Fourier transform; HALS, harmonic least squares; IGPVN, improvement of groundwater protection in Vietnam; MAR, managed aquifer recharge; NAWAPI, National Center for Water Resources Planning and Investigation, Vietnam; NGMN, National Groundwater Monitoring Network of Vietnam; OT_{SE}, ocean tide loading on the solid Earth; OT_{GW}, ocean tide loading on the aquifer's water; PSC, passive subsurface characterization; PT, pressure transducer; TSA, tidal subsurface analysis; VMD, Vietnamese Mekong Delta.

* Corresponding author.
E-mail address: felix.doerr@kit.edu (F. Dörr).

https://doi.org/10.1016/j.jhydrol.2025.133844
Received 18 February 2025; Received in revised form 11 June 2025; Accepted 5 July 2025
Available online 8 July 2025

their low elevation, and their high demand for freshwater often results in depleting groundwater heads, leading to sediment compaction and causing subsidence (Gambolati and Teatini, 2021). In light of climate change, global economic and population growth, and a resulting increase of groundwater demand and depletion, land subsidence hazards must be expected to exacerbate within the next decades (Herrera-García et al., 2021).

As one of the world's largest deltaic lowlands, the southern Vietnamese Mekong Delta (VMD) is a prominent example for hazardous land subsidence dynamics due to groundwater overexploitation, with rates of more than 3 cm a^{-1} (Erban et al., 2014; Minderhoud et al., 2017; Dörr et al., 2024). Other deltas and their metropolitan cities like the Ganges-Brahmaputra Delta (Dhaka), the Mississippi Delta (New Orleans), the Nile Delta (Alexandria) and the Yangtze Delta (Shanghai) are further examples for deltaic lowlands suffering from land subsidence (Syvitski et al., 2009).

Land subsidence due to groundwater depletion may be mitigated to some extent. However, the effectiveness of mitigation measures varies between the affected regions. In some previously subsiding regions like Tokyo and Osaka, Japan (Sreng et al., 2011), as well as Taipei, Taiwan (Chen et al., 2007), a significant land rebound followed a natural recovery of groundwater heads after a substantial reduction of groundwater extraction. Besides natural groundwater recharge, the injection of water or other fluids into the aquifer, e.g. in the context of managed aquifer recharge (MAR), may yield in significant land rebound, as achieved in the Wilmington oil field, California (Gambolati and Teatini, 2021). In other previously subsiding regions with limited rebound capability, a reduction of groundwater withdrawal substantially reduced further land subsidence, for example in Venice, Italy (Gambolati and Teatini, 2021) and in Shanghai, China (Zhang et al., 2015). In confined aquifer systems, such as in the VMD, the land rebound potential depends on elastic aquifer properties (Allen and Mayuga, 1970) which can be derived from groundwater head responses to harmonic forcings (Merritt, 2004; Cutillo and Bredehoeft, 2011; Rau et al., 2020).

The responses of groundwater heads to external forcings such as barometric pressure variations or ocean tides have been recognized and described long ago (Klönne, 1880; Veatch, 1906) and are used to derive hydro-geomechanical subsurface parameters since the 1940's (Jacob, 1940). Barometric pressure and ocean tides are subject to periodic variations, enabling an assessment of these effects not only in the time domain but in the frequency domain as well. This is equally valid for the response of groundwater heads to Earth tides (Bredehoeft, 1967). Earth tides are caused by small but effectful variations of gravitational potential due to the movement of celestial bodies, inducing motions in the solid Earth (Agnew, 2007). With the given knowledge of the movement of celestial bodies, Earth tide strains can be calculated for any location on the earth's surface and for any point in time.

Since decades methods in time and frequency domain have been developed and improved to derive hydro-geomechanical subsurface parameters like the specific storage S_s (m^{-1}) and the aquifer compressibility α (Pa^{-1}) from groundwater responses to Earth and atmospheric tides, well summarized by Turnadge et al. (2019) and framed by the terms passive subsurface characterization (PSC) and tidal subsurface analysis (TSA). Particularly in the context of land subsidence mitigation, coastal plains and deltaic groundwater bodies would benefit from the application of PSC methods, given that the elastic compressibility of the subsurface is a proxy for (i) the contribution of elastic aquifer compaction to the overall observed subsidence, (ii) the mitigation potential in terms of land rebound capability (Allen and Mayuga, 1970) and (iii) the elastic aquifer storage and therefore the capability to temporarily receive and store surplus water resources by deformation of the aquifer material (Bouwer, 2002).

This study aims to demonstrate the potential of PSC for assessing land subsidence mitigation in deltaic lowlands by estimating elastic geomechanical properties. The southern VMD serves as an ideal study area due to three key factors: (i) tidal signals in groundwater heads have not yet been systematically described in the region, (ii) high land subsidence rates and ongoing land loss necessitate an urgent evaluation of subsurface properties and processes, and (iii) the superposition of multiple harmonic forcings provides a unique opportunity to apply PSC in a complex setting influenced by various tidal drivers. While the application of previous PSC methods was restricted in near-coastal aquifers, the novel integration of ocean tide loading on the solid Earth enhances PSC-parameter estimations in such hydrogeological systems. Therefore, the findings of this study highlight the utility of PSC and its potential applicability to other deltaic aquifer systems.

2. Study area

2.1. Land subsidence and water resources in the southern Vietnamese Mekong Delta

The VMD and its adjacent metropolis Ho Chi Minh City (Fig. 1) are home to more than 21 million people (GSOV, 2024) who have been facing local land subsidence rates >3 cm a^{-1} for several years, amounting to an existential crisis (Erban et al., 2014; Minderhoud et al., 2017; Dörr et al., 2024). With an average elevation of only 80 cm above sea level measured in 2018 (Minderhoud et al., 2019), such high rates of subsidence require an urgent investigation of the process dynamics, parametrization of subsurface properties and the assessment of potential mitigation strategies. Intensive groundwater overexploitation, leading to a continuous decline in groundwater heads throughout the confined multi-aquifer-aquitard system (Duy et al., 2021) and thus increases the effective stresses in the aquifer and aquitard sediments, is considered to be the greatest single driver for land subsidence in the VMD (Minderhoud et al., 2020; Kondolf et al., 2022). In addition, the construction of upstream reservoirs, dams and hydropower plants, along with sand mining activities in the rivers and channels, cause a sediment deficit in the delta plain, contributing to the overall subsidence by failing to compensate non-anthropogenic subsidence due to natural compaction processes of the young delta sediments (Kondolf et al., 2022; Baldan et al., 2024). Moreover, anthropogenic infrastructure, such as urban settlements, bridges and roads exert a surplus load on the subsurface causing localized compaction (Neussner, 2019; Dörr et al., 2021).

The VMD socio-economic activities are highly dependent on water resources, as it is one of Southeast Asia's most productive areas in terms of agricultural and aquacultural food production (Van et al., 2023; Thong et al., 2010; Nguyen et al., 2019). Groundwater resources are extracted at up to half a million licensed and especially non-licensed extraction wells (Danh and Khai, 2015). With increasing trends of surface water salinization and pollution as well as more pronounced droughts, groundwater remains a water resource of major relevance in the VMD (Pham et al., 2023), which is unlikely to be replaced by other water resources in the near future. Therefore, a continuous decline in groundwater heads is anticipated, resulting in further expected land subsidence (Minderhoud et al., 2020).

Due to the low and flat topography, the hydraulic gradients in the rivers are low, enabling upstream propagation of ocean tides, resulting in tidal fluctuations of inland river water levels and salinity (Eslami et al., 2019). In an attempt to control such sea water intrusion and minimize its impact on the tributary channels, sluice gates were constructed in the southern VMD (Di Giusto et al., 2021; Hoanh et al., 2009; Nguyen, 2020), operated on seasonal or tidal scale. Fig. 1 illustrates the southern VMD with its rivers and channel infrastructure, the location of sluice gates in Ca Mau Province and the overall low topography of the VMD.

The VMD's hydrogeological units have been classified into seven aquifers and seven aquitards (Fig. 2). The top Holocene aquitard Q_2 is likely to prevent significant groundwater recharge by infiltration into the Holocene aquifer qh, particularly in the southern VMD, where it has

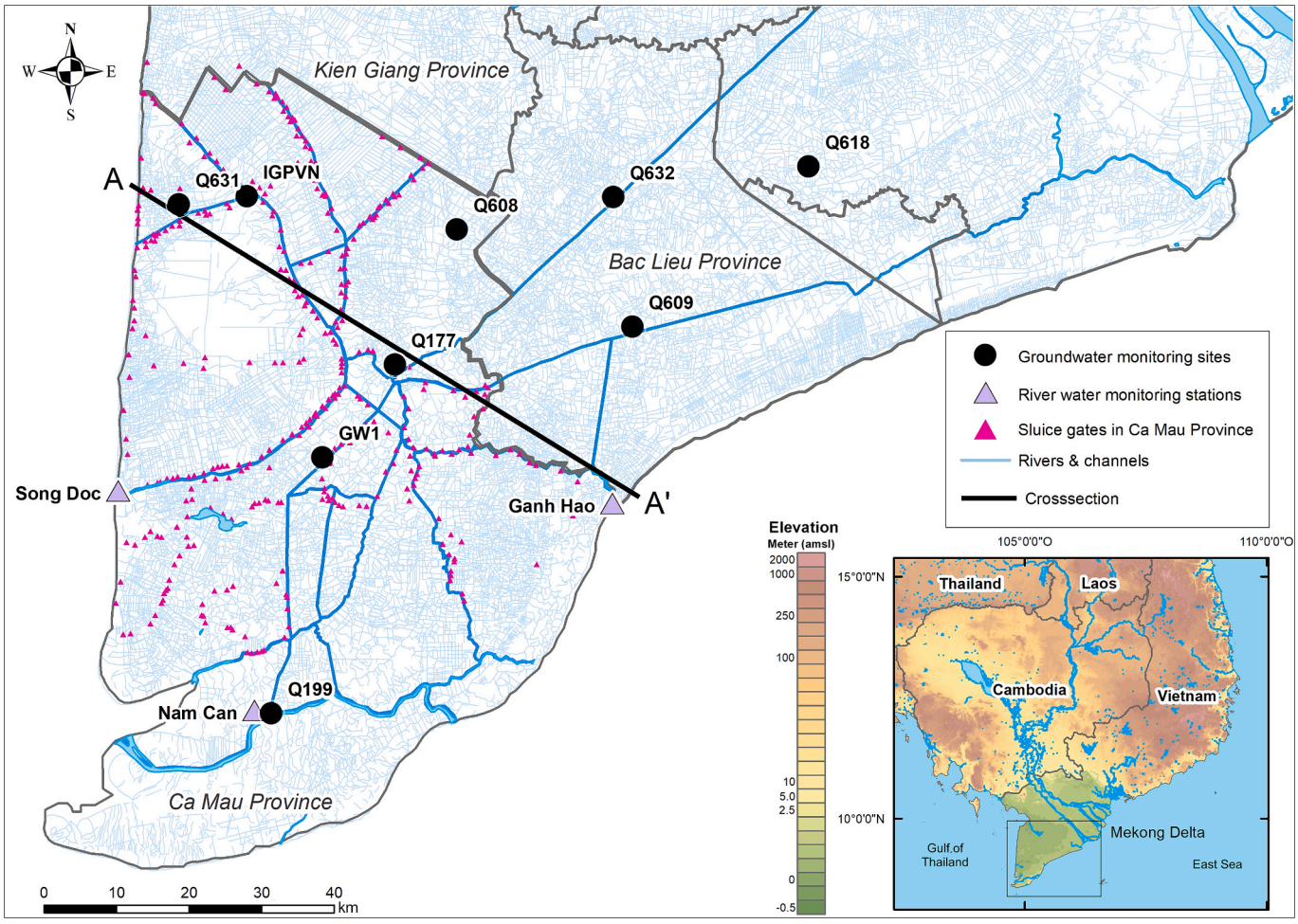

Fig. 1. Study area of the southern VMD, including the rivers and channels (bold and narrow blue lines), the location of the evaluated multi-depth groundwater and river water monitoring sites, and sluice gates in Ca Mau Province. Elevation data in the reference map are based on GTOPO30 (EROS, 2017) and locally for the VMD based on Minderhoud et al. (2019). (For interpretation of the references to color in this figure legend, the reader is referred to the web version of this article.)

a thickness of up to >20 m (Anderson, 1978; Pham et al., 2019; Bauer et al., 2022). At some locations, the qh aquifer is unconfined and hence capable of receiving groundwater recharge, for example, where sand dunes are present in the coastal provinces of Ben Tre, Tra Vinh and Soc Trang (Wagner et al., 2012). Early studies identified artesian conditions prior to significant anthropogenic groundwater extraction (Anderson, 1978), while ongoing groundwater monitoring in the last decade reveals depleting groundwater heads with rates of 0.01–0.55 m a^{-1} in the different aquifers (Duy et al., 2021). The upper, middle and lower Pleistocene aquifers qp_3, qp_{2-3} and qp_1 as well as the middle and lower Pliocene aquifers n_2^2 and n_2^1 and the upper Miocene aquifer n_1^3 are characterized by confined conditions. Fig. 2b illustrates a hydrogeological cross-section through the southern VMD, modified after Hoan et al. (2022). The introduced color code for the seven aquifers will be used henceforth in this study. The location of the cross-section line is marked in Fig. 1. In Fig. 2a, a detailed granulometry profile and the corresponding aquifer categorization of the IGPVN-monitoring site (location see Fig. 1) based on Pechstein et al. (2018) is presented. It shall be noted that the displayed granulometry of the Mesozoic basement (MZ) represents the crushed material rather than the undisturbed sediments. At that monitoring site, the aquifers n_2^1 and n_1^3 are not developed, and the development of the aquifers qh and qp_3 is not clearly distinguishable (Pechstein et al., 2018), indicated by the dashed blue section in the aquifer characterization in Fig. 2a.

2.2. Groundwater and surface water monitoring

The Vietnamese National Groundwater Monitoring Network (NGMN) provides a comprehensive dataset of groundwater head observations (i.e., as measured using well water levels) since the 1990s at numerous multi-depth monitoring sites in the VMD. Initially, these observations entailed manual measurements of groundwater heads on a daily to monthly basis. Since 2011, the NGMN has successively been enhanced by the installation of automated non-vented (i.e., absolute) pressure transducers (PTs) measuring groundwater heads at hourly resolution. The data obtained from the non-vented PTs is compensated for barometric pressure data recorded at each monitoring site by subtraction of the measured barometric pressure from the recorded absolute pressure (sum of water column and barometric loading) (NAWAPI, 2018).

The monitoring sites IGPVN and GW1 have been established by international research projects (IGPVN: Improvement of Groundwater Protection in Vietnam, Federal Institute for Geosciences and Natural Resources (BGR); GW1: ViWaT Engineering, Karlsruhe Institute of Technology (KIT)) complementing the NGMN-wells. At GW1, vented PTs were installed, at IGPVN non-vented PTs were replaced by vented PTs in 2021. Vented PTs are groundwater level sensors which are equipped with a venting tube that connects the submerged PT to the atmosphere, thus enabling a measurement of groundwater heads compensated for atmospheric pressure variations. Further clarification of the term barometric compensation as well as on measurement

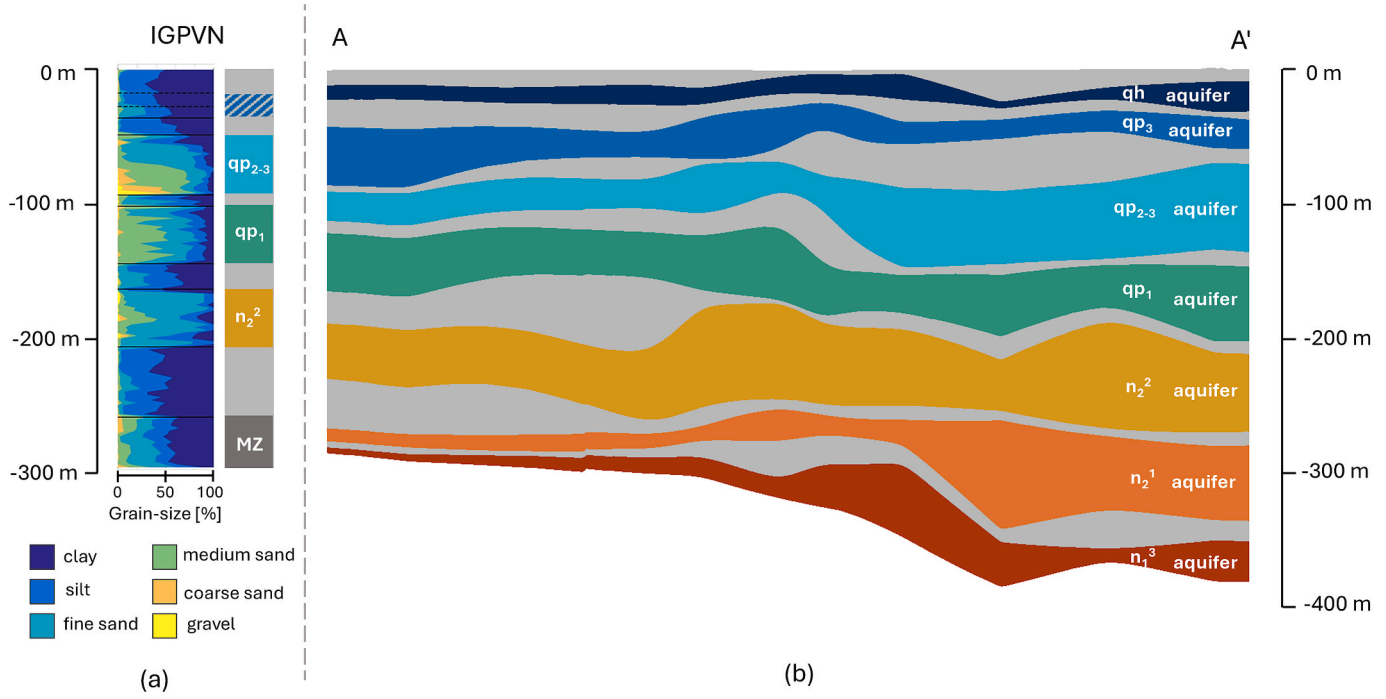

Fig. 2. Granulometry profile and aquifer-aquitard classification at the IGPVN monitoring site (Pechstein et al., 2018) (a) and hydrogeological cross section through the multi-layered aquifer-aquitard system of the southern VMD (Hoan et al., 2022) (b). The locations of the cross-section line and the IGPVN-monitoring site are marked in Fig. 1.

principles of vented and non-vented PTs is provided by Rau et al. (2019).

The IGPVN site comprises a total number of five observation wells, three of which are screened in the n_2^2 aquifer. For the observation wells IGPVN 1.3 ($qp_{2\text{-}3}$), IGPVN 1.2 (qp_1) and IGPVN 1 (n_2^2) data is available from 2016 until 2024, with one major gap of 13 months and several minor gaps. In n_2^2 aquifer two more observation wells IGPVN 1.1 and IGPVN 1.4 recorded groundwater heads from 2016 to 2020 with non-vented PTs. For an assessment of atmospheric loading at IGPVN, two different sources of barometric pressure data are available: (i) hourly barometric pressure records from the IGPVN site, which were also used for barometric compensation before 2021, when non-vented PTs were installed and (ii) hourly barometric pressure data from a meteorological station in Ca Mau City, situated in a distance of 30 km.

In the southern VMD, river water levels are recorded at three gauging stations: (i) Song Doc, located at the estuary of the Ong Doc river into the Gulf of Thailand in approximately 2 km distance to the coast, (ii) Ganh Hao, located at the estuary of the Ganh Hao river into East Sea in approximately 1 km distance to the coast and (iii) Nam Can, located in Nam Can Town in the Cửa Lớn river, a connecting river between the Gulf of Thailand and the East Sea.

In this study, groundwater head data of 35 NGMN wells from seven stations covering six different aquifers are used, as well as of five wells at IGPVN and three wells at GW1. Additionally, records of groundwater extraction rates from a municipal water supply well (G22) in Ca Mau City between December 2023 and January 2024 were provided by the Vietnamese National Center for Water Resources Planning and Investigation (NAWAPI). The location of the groundwater and river water monitoring stations used in this study are illustrated in Fig. 1.

3. Methods

3.1. Frequency analysis

To evaluate the response of groundwater heads to Earth tides, atmospheric tides, ocean tides or river tides, the underlying frequency patterns in the respective time series are analyzed by two independent methods: (i) the Fast Fourier Transform (FFT) and (ii) the harmonic least-squares (HALS) estimation. In FFT analyses, a given time series is decomposed into a linear sum of sinusoidal functions (Acworth et al., 2016), so that the Fourier transform $\mathscr{F}$ of the input signal $s(t)$ reads as

$$\hat{s}(f_k) = \mathscr{F}\{s(t_n)\} = \sum_{n=0}^{N-1} s(t_n) e^{-\frac{2\pi i k n}{N}} \tag{1}$$

where N is the number of observations, k is the frequency index, i is the imaginary unit, n the time index and

$$f_k = k f_s / N \tag{2}$$

with f_s as the sampling rate of the dataset. An alternative approach for the extraction of harmonic components is the application of a harmonic least squares (HALS) estimation (Agnew, 2007):

$$\min_{a_c, b_c} \sum_{n=1}^{N} \left[y_n(t_n) - \sum_{c=1}^{C} \left[a_c \cos(2\pi f_c t_n) + b_c \sin(2\pi f_c t_n) \right] \right]^2 \tag{3}$$

where N is the number of observations, t_n the time, and $y_n(t_n)$ the corresponding observation value, C is the total number of investigated harmonic components c, f_c is the frequency and a_c and b_c are the fitting coefficients.

Both methods yield in complex numbers, which can be decomposed into values of amplitude and phase for the considered frequency. The utilization of complex numbers $\hat{z}$ proves advantageous in the context of PSC analyses, as they encompass information on both the amplitude z and the phase shift ϕ. With the Eq. (4 [1-3]) any of the three values can be calculated from the other two:

$$\hat{z} = z \cdot e^{i\phi}; \quad \phi = \arg\hat{z}; \quad z = abs(\hat{z}) \tag{4 [1-3]}$$

The two methods vary in the requirement of input data quality, as FFT requires continuous data whereas HALS is capable of handling gaps (Schweizer et al., 2021). While FFT yields in amplitude spectra at a fine and constant frequency discretization f_k, HALS takes only predefined frequencies into consideration. Consequently, significant variations

between calculated FFT and HALS amplitudes may suggest that for the HALS analysis, not all relevant frequencies were considered. In this study, for any performed frequency analysis, both methods were applied for validation purposes. HALS outperforms FFT in terms of accuracy in amplitude and phase estimation and therefore is preferable to FFT in PSC (Schweizer et al., 2021). Thus, the amplitudes and phases obtained from HALS were used for the PSC-parameter estimations in this study. For the HALS analyses in this study, the ten most commonly investigated frequencies in groundwater analysis as listed in Table 1 were considered. In tidal analysis, frequencies with near-diurnal periodicity are commonly denoted in cycles per day (cpd).

For the FFT analyses, gaps were filled with an autoregression algorithm (*fillgaps*, MATLAB, 2023), which takes the frequency patterns within the datasets into consideration. To minimize the impact of interpolation on FFT results, subsets of the complete datasets with few or no gaps were selected. The subset durations vary between 0.4 and 5.1 years with an average of 3.1 years. After the selection of groundwater sub-datasets mostly minor gaps of a few hours, e.g. as caused by bi-annual groundwater sampling campaigns, remained and required interpolation. A summary of the subset employed for the frequency analyses and a visualization of the respective time series is provided in the Supplementary information. At all wells >99 % of the data utilized in the FFT analyses is original data with <1 % of interpolated values.

The analyzed river water levels were measured at irregular intervals, on average approximately 6 times per day, requiring an interpolation of a greater fraction of the dataset to obtain a dataset of hourly resolution and thus a more careful comparison of FFT and HALS based amplitudes in the frequency analyses.

3.2. Calculation of Earth and ocean tide strains

Volumetric Earth tide strains, denoted in nanostrain (nstr), were calculated at hourly resolution using *PyGTide* (Rau et al., 2022b), a Python wrapper for *ETERNA PREDICT 3.4* (Wenzel, 1996). Ocean tides may affect tidal signals in inland groundwater heads by two independent processes: (i) by ocean tide loading on the solid Earth (Agnew, 2012), further denoted as OT_{SE}, and (ii) by ocean tide loading on the aquifer's water (Jacob, 1950; van der Kamp, 1972), further denoted as OT_{GW}. OT_{SE} causes strain waves, which propagate from the ocean coast towards the inland by the geologic media, while OT_{GW} is a pressure wave that propagates from the ocean coast towards the inland by the liquid phase (pore water) only. The volumetric strains due to OT_{SE} are calculated with the Fortran-based software package *SPOTL* (Agnew, 2012) at hourly resolution. For an aquifer, which extends below the seabed, the amplitude damping of OT_{GW} in a coastal aquifer can be calculated with Eq. (5) (van der Kamp, 1972):

$$A_{gw}(x) = \frac{1}{2} A_{sw} \gamma e^{-\sqrt{\frac{\pi S_s}{K t_0}} x} \tag{5}$$

where A_{gw} (m) and A_{sw} (m) are the amplitudes in the groundwater and seawater respectively, x (m) is the distance to the shoreline, γ (−) is the uniaxial loading efficiency, t_0 is the tidal period (s), equal to the inverse of the frequency f_c, S_s (m^{-1}) and K ($m\ s^{-1}$) are the specific storage and the hydraulic conductivity of the considered aquifer. Given that the Gulf of Thailand is relatively shallow with an average depth of 45 m, and a maximum depth of 83 m (Aungsakul et al., 2007; Siripong, 1985), it can be reasonably assumed that the investigated aquifers with depths of 101–142 m and 161–202 m respectively at IGPVN extend below the seabed, allowing the application of Eq. (5) for the IGPVN monitoring site.

Table 1
Summary of the ten most relevant frequencies in groundwater analysis after Merritt (2004), McMillan et al. (2019) and Rau et al. (2020).

Darwin name	Frequency (cpd)	Earth Tides	Atmospheric Tides	Ocean and River Tides
Q_1	0.893244	Yes	–	Yes
O_1	0.929536	Yes	–	Yes
M_1	0.966446	Yes	–	Yes
P_1	0.997262	Yes	Yes	Yes
S_1	1.000000	–	Yes	–
K_1	1.002738	Yes	Yes	Yes
N_2	1.895982	Yes	–	Yes
M_2	1.932274	Yes	–	Yes
S_2	2.000000	Yes	Yes	Yes
K_2	2.005476	Yes	Yes	Yes

For the evaluation of the groundwater response to the total volumetric strain caused by OT_{SE} and Earth tides, the two strain time series can be added up to a single time series prior to the conducted frequency analysis. Alternatively, if the well water level response to Earth and ocean tide strains shall be disentangled, the two time series can be considered separately. In accordance with the harmonic addition theorem (Arfken and Weber, 2005), the amplitudes and phases obtained from the merged time series of Earth tides and OT_{SE} (denoted as the complex number $\hat{z}_{f_c}^{\{\mathrm{ET+OT}_{SE}\}}$) equals the sum of the separately calculated amplitudes and phases (each denoted as the complex numbers $\hat{z}_{f_c}^{\mathrm{ET}}$ and $\hat{z}_{f_c}^{\mathrm{OT}_{SE}}$):

$$\hat{z}_{f_c}^{\{\mathrm{ET+OT}_{SE}\}} = \hat{z}_{f_c}^{\mathrm{ET}} + \hat{z}_{f_c}^{\mathrm{OT}_{SE}} \tag{6}$$

It shall be noted here that, depending on the phase shift, amplitudes of Earth tides and OT_{SE} could either add up or counteract each other by causing constructive or destructive interference of the sinusoidal signals.

3.3. Disentanglement of Earth, ocean and atmospheric tides

For the determination of the barometric efficiency *BE* in the frequency domain, the response of groundwater heads to atmospheric tides at S_2 is evaluated. Given that S_2 is present in Earth, ocean and atmospheric tides (Table 1), the S_2 signal in the measured groundwater observation data $\hat{z}_{S_2}^{\mathrm{GW}}$ must be disentangled into its Earth and ocean tide component $\hat{z}_{S_2}^{\mathrm{GW}\cdot\{\mathrm{ET+OT}_{SE}\}}$ and its atmospheric component $\hat{z}_{S_2}^{\mathrm{GW}\cdot\mathrm{AT}}$. Eq. (7) is an adaptation of the formulation by Rau et al. (2020) under additional consideration of ocean tide strains:

$$\hat{z}_{S_2}^{\mathrm{GW}\cdot\mathrm{AT}} = \hat{z}_{S_2}^{\mathrm{GW}} - \hat{z}_{S_2}^{\mathrm{GW}\cdot\{\mathrm{ET+OT}_{SE}\}} = \hat{z}_{S_2}^{\mathrm{GW}} - \frac{\hat{z}_{M_2}^{\mathrm{GW}}}{\hat{z}_{M_2}^{\{\mathrm{ET+OT}_{SE}\}}} \hat{z}_{S_2}^{\{\mathrm{ET+OT}_{SE}\}} \tag{7}$$

The hat denotation indicates complex numbers. After the disentanglement of Earth, ocean and atmospheric tide signals, the barometric efficiency based on the S_2 response of groundwater heads to atmospheric tides $BE_{S_2}^{AT}$ can be calculated after Rau et al. (2020) with Eq. (8) as:

$$\mathrm{BE}_{S_2}^{\mathrm{AT}} = \frac{1}{A_{S_2}^{r}} \mathrm{abs}\left[\frac{\hat{z}_{S_2}^{\mathrm{GW}\cdot\mathrm{AT}}}{\hat{z}_{S_2}^{\mathrm{AT}}}\right] \tag{8}$$

with the amplitude response $A_{S_2}^{r}$ between well water levels and the actual aquifer pore pressure. $A_{S_2}^{r}$ is a function of well and aquifer parameters and can be calculated by using the python package *HydroGeoSines* (HGS, 2023).

3.4. Calculation of formation compressibility and specific storage

In unconsolidated systems like the sedimentary aquifers of the southern VMD, grain compressibility can commonly be neglected as it is much smaller than bulk compressibility (Rau et al., 2022a), so the uniaxial loading efficiency γ (−) and the barometric efficiency *BE* (−) can be expressed with Eq. (9) when undrained conditions are considered for the hydraulic head oscillation at subdiel frequencies (1–2 cpd) (Acworth et al., 2016; Jacob, 1940; van der Kamp and Gale, 1983):

$$BE = 1 - \gamma = 1 - \frac{\alpha}{\theta \cdot \beta + \alpha} \quad (9)$$

α as the formation compressibility (Pa^{-1}), β as the water compressibility ($4.59 \cdot 10^{-10}$ Pa^{-1} at 20 °C for water) and θ (−) as the aquifer porosity. Consequently, once BE and θ have been defined, the compressibility α can be calculated. By considering α as the drained compressibility, the specific storage S_s can be calculated with Eq. (10) (Cooper, 1966; Acworth et al., 2016):

$$S_s = \rho_w g(\theta \cdot \beta + \alpha) \quad (10)$$

ρ_w as the water density (kg m^{-3}) and g as the gravity constant (m s^{-2}) and the assumption of incompressible grains.

Forced by harmonic drivers like Earth or atmospheric tides, a flow between the aquifer and well is induced, that can be used to derive subsurface parameters including the specific storage S_s (Rojstaczer, 1988; Bredehoeft, 1967; Hsieh et al., 1987). Analytic solutions for such groundwater flow problems have been derived for confined conditions (Hsieh et al., 1987) and semi-confined conditions (Rojstaczer, 1988) as a function of well and aquifer parameters, which can be calculated with the python package *HydroGeoSines* (HGS, 2023). The sign of M_2 phase shift $\Delta\phi_{M_2}$(°) between Earth tides and groundwater heads bares information about the flow condition in the absence of borehole skin effects (Valois et al., 2022). For example, a positive M_2 phase shift is indicative of vertical flow as given in the presence of vertical drainage from an overlying aquitard. Conversely, a negative M_2 phase shift could indicate horizontal flow in and out of the well, suggesting fully or semi-confined conditions (Rojstaczer, 1988; Rau et al., 2020; Roeloffs et al., 1989; Xue et al., 2016; Valois et al., 2022). This differentiation, derived from considerations of Earth tides as single drivers for subsurface strains, is equally applicable regardless of the total volumetric strain's origin, i.e., the sum of Earth tide strains and OT_{SE}.

The compaction η (m) of a single confined aquifer can be calculated as the product of the aquifer thickness b (m), the compressibility α (Pa^{-1}), and the change in the effective intergranular stress $\Delta\sigma_z$ (Pa) (Gambolati and Teatini, 2021) to:

$$\eta = b \cdot \alpha \cdot \Delta\sigma_z \quad (11)$$

where $\Delta\sigma_z$ can be calculated from the piezometric decline of water level in the confined aquifer Δz (m) to:

$$\Delta\sigma_z = \rho_w \cdot g \cdot \Delta z \quad (12)$$

3.5. Identification of dominant drivers

For assessing the dominant drivers for the tidal signals in groundwater heads, the S_2 and M_2 ampltiude values as well as the ratio of S_2 and M_2 amplitudes are considered. Given that the S_2 amplitude in atmospheric tides is commonly below 15 mm (Ray and Ponte, 2003) and the diurnal M_2 and S_2 amplitudes in groundwater responses to Earth tides are commonly in a range of maximum 10–20 mm (Bredehoeft, 1967), S_2 and M_2 amplitudes significantly beyond these ranges indicate the presence of additional drivers. In the presence of dominant ocean or river tide loading, the S_2 and M_2 amplitudes in groundwater heads are expected to exceed the aforementioned ranges and occur in a ratio close to that of the driver's amplitudes (Patton et al., 2021). If the groundwater heads are characterized by high S_2 and low M_2 amplitudes, ocean or river tides are unlikely to be the dominant drivers, indicating that other drivers are at play.

3.6. Summary of workflow and applied methods

The presented study utilizes time series of observed groundwater heads, computed subsurface strains due to Earth tides and ocean tide loading on the solid Earth (OT_{SE}), observed barometric pressure, inland river water levels, ocean water levels (derived from estuary river water level observations) as well as groundwater extraction rates and pumping well water level dynamics, for comprehensive frequency analyses. The identified amplitude characteristics of groundwater observation wells are discussed as evidence for the presence of loading signals in groundwater head timeseries. The ratio of M_2 and S_2 amplitudes are used to identify groundwater head timeseries where ocean tides, river tides or groundwater extraction dominate the groundwater amplitude spectra. After a site-specific assessment of potential further forcings, the S_2 signal in groundwater is disentangled into its barometric-, Earth tide- and OT_{SE}–components at a selected groundwater monitoring site. Based on that, the elastic specific storage is derived and discussed as a proxy for elastic compaction, water storage and land rebound potential in the context of land subsidence mitigation measures. Fig. 3 presents a flow chart of the study's methodological approach.

4. Results

4.1. Tidal signals in groundwater and surface water levels

A regional frequency analysis of groundwater heads reveals the presence of distinct amplitudes at characteristic frequencies like S_2 and M_2 with varying intensity. Fig. 4 summarizes the FFT amplitude spectra annotated with HALS amplitudes of the regional frequency analysis, calculated with Eqs. (1)–(3). The analysis shows a good agreement between the HALS-based and FFT-based calculated S_2 and M_2 amplitudes. Note that individual tidal components surrounding 1.00 cpd are not attributed to a specific frequency (e.g., S_1, P_1 and K_1) as they are too close to each other (Table 1) and a differentiation between these frequencies is not considered in this work.

The frequency analyses of recorded river water levels from Ganh Hao (Fig. 5a), Nam Can (Fig. 5b) and Song Doc (Fig. 5c) reveal distinct tidal signals at all three gauging stations with unique amplitude distributions. At Ganh Hao, the tidal regime is characterized by dominant semi-diurnal frequencies with an M_2 amplitude of 925 mm and a K_1 amplitude of 649 mm (Fig. 5a-III). In contrast, at Song Doc, the amplitude at the diurnal frequency K_1 is most pronounced with 226 mm, while the amplitude at the semi-diurnal frequency M_2 is with 111 mm lower (Fig. 5c-III). At Nam Can, the tidal regime is characterized by M_2 amplitudes of 603 mm and K_1 amplitudes of 455 mm (Fig. 5b-III).

Due to the superposition of two different ocean tide regimes from the East Sea and the Gulf of Thailand, Nam Can is characterized by a distinct and unique amplitude distribution which noticeably differs from Ganh Hao and Song Doc. For all three datasets, the HALS-based amplitudes (considering only the irregularly measured raw data) and the FFT-based amplitude spectra (considering the hourly interpolated data) show a good agreement, suggesting that the interpolation of gaps (Fig. 5a-II–c-II) represent the actual river water level dynamics well.

4.2. Characterizing the drivers of tidal signals in groundwater heads

In a preliminary assessment of the dominant drivers of the tidal signals in groundwater heads, the M_2 and S_2 amplitudes obtained from the HALS analyses are summarized in Fig. 6. This preliminiary assessment indicates that the M_2 and S_2 amplitudes of the majority of wells are below 10 mm and thus comply with the range commonly found within impact of Earth tides of approximately maximum 10–20 mm (Bredehoeft, 1967) and atmospheric tides of approximately 15 mm (Ray and Ponte, 2003). However, the potential influence of river or ocean tides, as well as potentially periodic groundwater extraction patterns, cannot be excluded for those locations without a site-specific assessment of the local conditions. In contrast, the M_2 and S_2 amplitudes at the observation wells at the monitoring site Q199, as well as at two observation wells at the monitoring site Q177 and one monitoring well at IGPVN exceed the typical ranges of amplitude responses for Earth and atmospheric tides (Bredehoeft, 1967; Ray and Ponte, 2003), indicating the presence of additional tidal forcings.

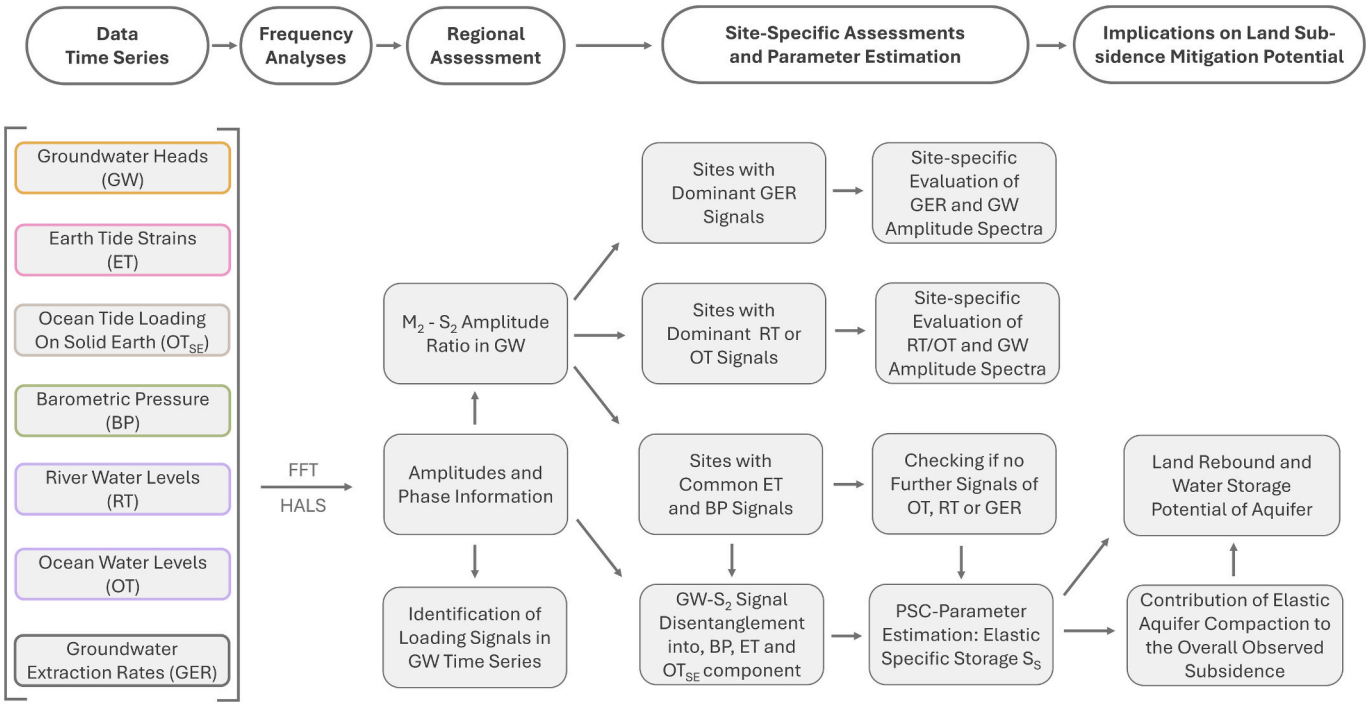

Fig. 3. Overview of the datasets and the workflow that was applied to evaluate and disentangle tidal loading signals and reveal geomechanical properties of the coastal groundwater system in the southern VMD.

At the monitoring sites Q177 and IGPVN some observation wells exhibit uncharacteristically high S_2 amplitudes, while the M_2 amplitudes do not exceed the typical response to Earth tides, indicating that an additional forcing without a M_2 frequency is at play. For those wells, a detailed assessment of the observed groundwater heads in the time domains reveals that the water level fluctuations are induced by periodic groundwater extraction patterns. Q177 is located in 475 m distance to a municipal water supply well (G22) screened in $n2^2$ aquifer, which operates at scheduled intervals. Fig. 7d illustrates the evident correlation of groundwater head variations at Q177 in the $n2^2$ aquifer and the groundwater extraction patterns from G22 (also from $n2^2$ aquifer), characterized by a recovery of groundwater heads in the night, when the operation of the water supply wells is paused. It shall be noted here that the apparent lead of groundwater drawdown and recovery of 3 h compared to the extraction rates in Fig. 7d is considered to be due to a time offset in one of the two recorded datasets.

Fig. 7e visualizes the recorded groundwater heads in the pumping well G22 for the available four-weeks interval between December 2023 and January 2024 showing a drawdown of 4.0 m when the pumping well is operated. The FFT-amplitude spectra of the groundwater heads in the pumping well G22 and in the observation well at Q177 are visualized in Fig. 7f, showing a similar frequency response of both wells, characterized by amplitude peaks at harmonics of S_1 at multiples of 1.00 cpd.

Fig. 7b shows that for the observation well at Q177 in $n2^2$ aquifer, in February and May 2018, the overall groundwater fluctuation magnitude drops from approximately 0.6 m–0.2 m. A similar temporal variation can be observed in qp_1 aquifer at Q177 (Fig. 7c), where between January and May 2022 the overall groundwater fluctuation magnitude is temporarily low and shows a sudden increase after May 2022. This incontinous magnitude in the well water level fluctuations at Q177 in qp_1 and $n2^2$ indicate the presence of anthropogenic influence on the well water level fluctions.

Similarly, the periodic groundwater head variations in the observation well IGPVN 1.2 (qp_1) can be considered to be induced by periodic groundwater extraction patterns of a local water supply well, which is located in 820 m distance, screened in qp_1 aquifer with a licensed pumping rate of 275 $m^3\ d^{-1}$ (Pechstein et al., 2018). Pechstein et al. (2018) had concluded too, that groundwater extraction patterns are the drivers for the strong water level fluctuation in IGPVN 1.2, substantiated by an evaluation of water level variations during a short power blackout, when the water supply well's operation paused off schedule. The close-up visualization of IGPVN 1.2 (qp_1) in Fig. 10f-II underlines that the fluctuations of groundwater heads are caused by non-natural drivers, showing an irregular temporal variation which cannot be attributed to natural processes like Earth and atmospheric tide forcings.

The preliminary assessment of potential drivers (Fig. 6) suggests that ocean or river tide loading are dominant at Q199, given that both, M_2 and S_2 amplitudes exceed the range of common groundwater response to Earth or atmopheric tides. A site-specific analysis reveals that the monitoring site Q199 in Nam Can town is located in less than 100 m distance to the Cửa Lớn river (Fig. 8c). A comparison of the amplitude spectra of groundwater and river water levels (Fig. 8a and b) shows a clear correlation with an average ratio of 1:0.16 between water level amplitudes in the river and in the observation well (Fig. 8d).

4.3. *Disentanglement of well water level responses to harmonic forcings*

In a first step, the presence of OT_{GW} is assessed with Eq. (5) for the monitoring site IGPVN, considering the site's distance to the coast of $x = 15$ km, as well as a hydraulic conductivity and specific storage of $1.1 \cdot 10^{-4}$ m s^{-1} and $6.3 \cdot 10^{-6}$ m^{-1} respectively for the $n2^2$ aquifer (Pechstein et al., 2018). A loading efficiency of $\gamma = 1$ is assumed, to calculate the maximum of expectable OT_{GW} under consideration of the aforementioned parameters. The ocean tide amplitudes (Fig. 9a) were derived from the amplitude spectrum at Song Doc (Fig. 5c-III), representing a good proxy for the ocean tides in the Gulf of Thailand due to its close vicinity to the coast and its good agreement with general tidal characterization of the Gulf of Thailand (Aungsakul et al., 2007; Cui et al., 2019).

Fig. 9b shows the damping of the three strongest ocean tide amplitudes at M_2, K_1 and O_1 frequency, yielding in insignificant OT_{GW} amplitudes (<0.01 mm) at 6.4 km inland and thus being negligible at IGPVN, located 15 km inland. On the contrary, OT_{SE} is not negligible at IGPVN with a volumetric strain amplitude of 2.0 nstr at M_2 (Fig. 10b-III

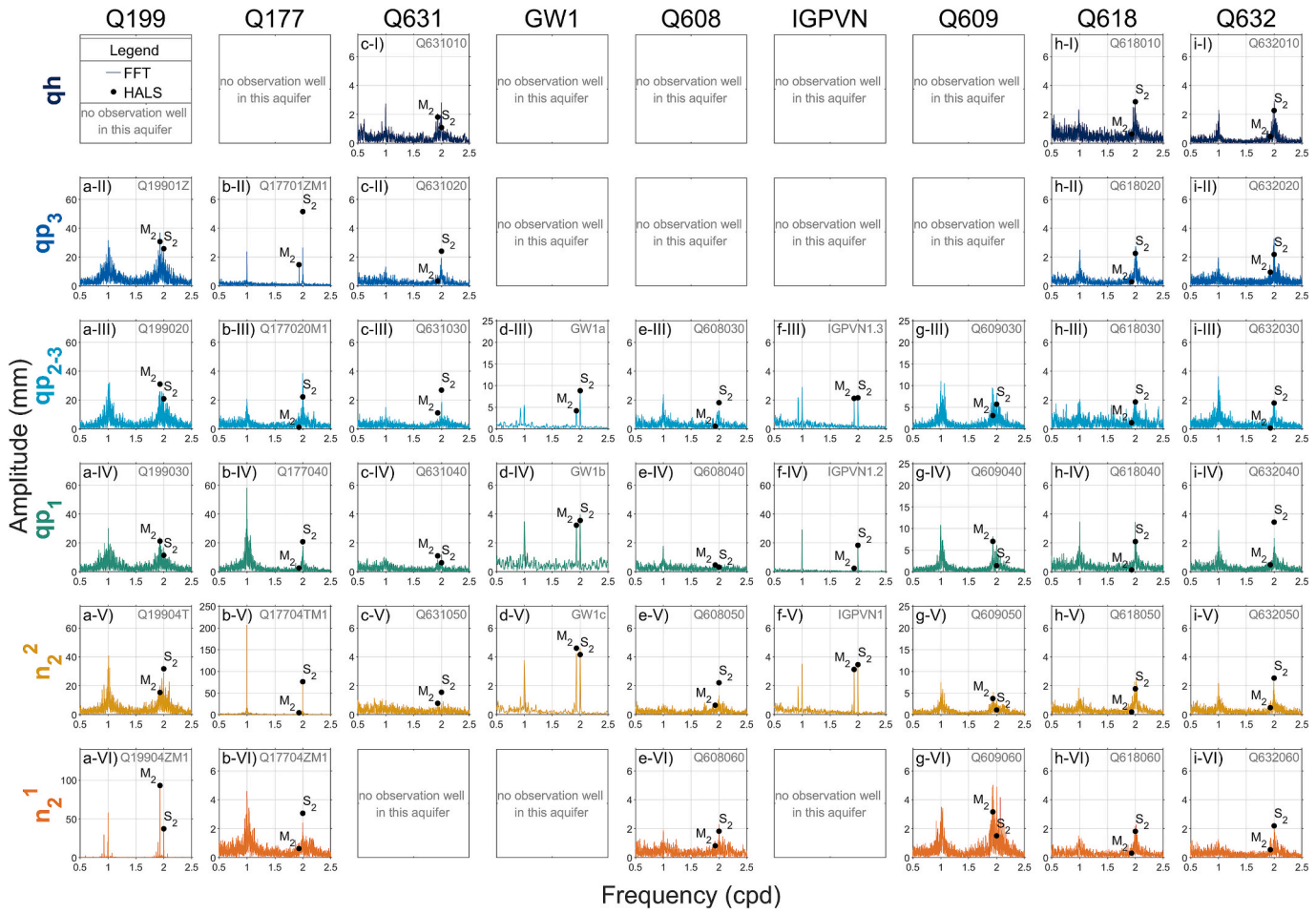

Fig. 4. Frequency analysis of 41 well water level time series in the southern VMD with FFT amplitude spectra (lines) and HALS amplitudes (calculated for the 10 frequencies listed in Table 1, displayed for M_2 and S_2 frequency as dots). The location of the nine multi-depth monitoring sites is shown in Fig. 1. It should be noted that the visualization encompasses distinct y-axis categories, namely 7.5 mm, 25 mm, 75 mm, 125 mm and 250 mm.

and b-IV). For IGPVN, no water level data of rivers or channels in the vicinity is available. Given that the site is located at the border of the freshwater area of U-Minh and the nearby channels are protected from saltwater intrusion and tidal propagation by sluice gates (Fig. 1), river tides are considered as negligible drivers for groundwater heads at IGPVN in this study.

All analyzed data are presented in Fig. 10a-I–i-I, comprising volumetric Earth tide strains (Fig. 10a-I), volumetric strains due to OT_{SE} (Fig. 10b-I), barometric pressure (Fig. 10d-I) and groundwater heads in five observation wells, screened in three aquifers (Fig. 10e-I–i-I). A close-up visualization of the data for a 12-day period in Fig. 10a-II–i-II illustrates the periodic character of each dataset. From a comparison of the measured groundwater heads in the three aquifers (Fig. 10e-II–i-II) no significant effect of the periodic groundwater extraction from qp_1 can be inferred in the adjacent aquifers. Fig. 10a-III–i-III and a-IV–g-IV illustrate the amplitude spectra for 2018 (with non-vented PTs) and 2023 (with vented PTs), both periods are marked in grey in Fig. 10a-I–i-I.

The calculated M_2 amplitudes and phases of the individual volumetric strains due to Earth tides and OT_{SE} as well as their sum are visualized in Fig. 11. The additional consideration of OT_{SE} yields in an increase of the total volumetric strain amplitude at M_2 from 17.0 nstr to 18.6 nstr and a phase shift of 3.6° compared to a consideration of Earth tide strains only.

4.4. Estimation of specific storage and compressibility

For the calculation of the barometric efficiency *BE*, atmospheric tides were disentangled from Earth and ocean tides with Eq. (7) for the monitoring site IGPVN. $A^r_{S_2}$ was calculated to $A^r_{S_2} > 0.99$ for all assessed well water level time series, indicating an insignificant difference between well water levels and pore pressure heads in the surrounding aquifer. The calculated barometric efficiency for the non-vented and vented dataset of observation wells yields in consistent results with $BE = 0.19 \pm 0.02$ in n_2^2 aquifer. Calculation results for the observation well in $qp_{2\text{-}3}$ vary between $BE = 0.12$ and $BE = 0.19$ for the assessed periods of 2018 (non-vented) and 2023 (vented).

In 2023, the phase shift between $BE^{AT}_{S_2}$ in $qp_{2\text{-}3}$ aquifer and the atmospheric driver is with 17° (Fig. 12b-II) significantly greater than the respective phase shift in all four assessed observation wells in 2018 (Fig. 12b-I). For the observation well in qp_1, $BE^{AT}_{S_2}$ was not calculated, given that the S_2 amplitude in groundwater heads is distorted significantly by anthropogenic groundwater extraction patterns (Fig. 7). The calculated barometric efficiency $BE^{AT}_{S_2}$ is summarized in Table 2, alongside with the M_2 amplitude response to Earth tide strains and OT_{SE} (denoted as A_{M2}) and the respective phase shift $\Delta\phi_{M2}$. In Fig. 12 the results are visualized as polar plots.

The M_2 amplitude responses to volumetric strains reveal a variation of 6 % ($\Delta = 0.006$ mm/nstr) at IGPVN 1.3 ($qp_{2\text{-}3}$), 13 % ($\Delta = 0.014$ mm/nstr) at IGPVN 1.2 (qp_1) and 3 % ($\Delta = 0.004$ mm/nstr) at IGPVN 1 (n_2^2) between the vented and non-vented periods, 2018 and 2023. For the calculated *BE*, the variation between the vented and non-vented dataset is 7 % ($\Delta = 0.014$ mm/mm) at IGPVN 1. Given the uncharacteristically high S_2 phase shift of 17° (Fig. 12b-II), the calculated *BE* at IGPVN 1.3 is

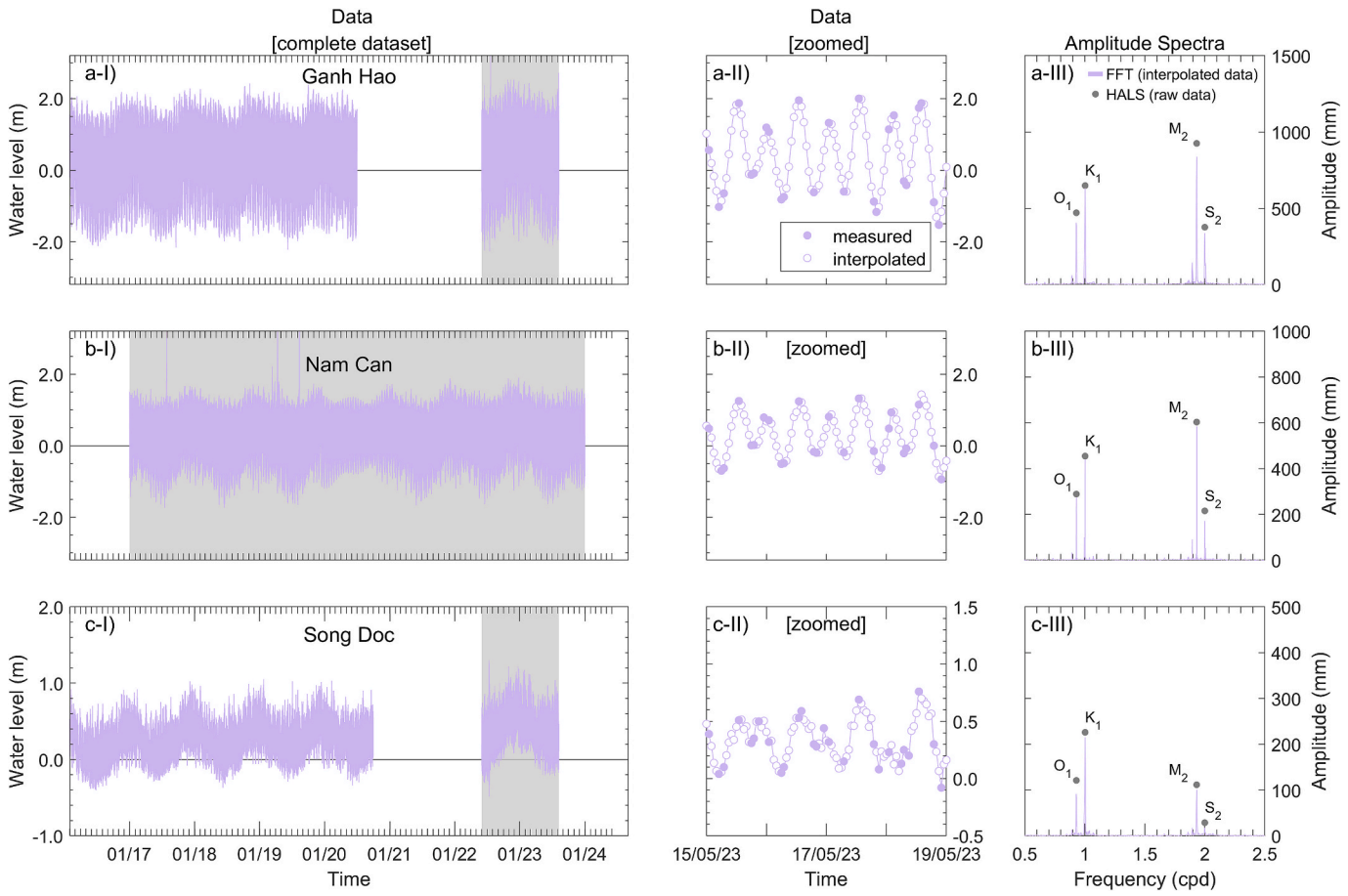

Fig. 5. Frequency analysis of river water levels at Ganh Hao (a), Nam Can (b) and Song Doc (c), including a visualization of the measured river water levels between 2016 and 2024 (I), a close-up visualization of a 4-day period (II), FFT amplitude spectra (lines), and HALS amplitudes (calculated for the 10 frequencies listed in Table 1, displayed for O_1, K_1, M_2 and S_2 frequency as dots) (III). The time periods used for the frequency analyses are highlighted in grey in (I) and were chosen according to the gaps and measurement frequencies in the datasets.

considered to be afflicted by the periodic groundwater extraction patterns in qp_1 and therefore not representative for a comparison. The calculation results indicate a positive M_2 phase shift of 0.9° for IGPVN 1.2 in qp_1 for 2023 (vented) while it was negative in 2018 (non-vented) (Fig. 12a-I and a-II).

The calculated M_2 phase shift between groundwater heads and volumetric strains due to Earth tides and OT_{SE} is negative in $qp_{2\text{-}3}$ and n_2^2 aquifer, indicating horizontal flow between well and aquifer to be dominant. For such flow conditions, the analytical solution of Hsieh et al. (1987) can be applied to calculate the specific storage S_s from well water level responses to volumetric strains without a requirement of a priori information on porosity. This method was applied as implemented in *HydroGeoSines* (HGS, 2023).

At IGPVN, the porosity in $qp_{2\text{-}3}$ and n_2^2 aquifer was determined to $\theta = 0.33$ for both aquifers based on grain size analysis in previous studies (Pechstein et al., 2018). The availability of porosity data allows an alternative calculation of α and S_s based on *BE* with Eqs. (9) and (10). The calculation results for S_s after Hsieh et al. (1987) are summarized in Table 3 alongside the calculation results of S_s based on *BE* with Eqs. (9) and (10). The difference in the S_s estimates of these two passive methods is small (Table 3). More importantly, the results of both passive methods ($5.9\text{–}7.8 \cdot 10^{-6}$ m^{-1}) comply well with S_s estimates from a pumping test conducted independently in the n_2^2 aquifer ($6.3 \cdot 10^{-6}$ m^{-1}, refer to Pechstein et al., 2018). While no hydraulic test was available for the $qp_{2\text{-}3}$ aquifer, the results comply well with regional aquifer parametrization of the study area (DWRPIS, 2010; Pechstein et al., 2018).

From the results in Table 3, the elastic compressibility can be calculated with Eq. (10) as $\alpha = 6.4\text{–}7.5 \cdot 10^{-10}$ Pa^{-1} in $qp_{2\text{-}3}$ and $\alpha = 4.5\text{–}6.4 \cdot 10^{-10}$ Pa^{-1} in n_2^2 aquifer. With thicknesses of $b = 41$ m of each aquifer (Pechstein et al., 2018), an elastic compaction (rebound) η of 0.18–0.30 mm per depletion (recovery) of hydraulic head $\Delta z = 1$ m can be derived for the two considered aquifers from Eqs. (11) and (12).

5. Discussion

5.1. Identification of tidal signals and loading imprints

As shown in the regional frequency analysis presented in Figs. 4 and 6, the groundwater heads in all assessed observation wells in the southern VMD respond to natural forcings, i.e. at M_2 and S_2 frequencies. In the study area, these tidal signals can be attributed to ubiquitous signals of atmospheric loading and Earth tide strains as well as site-specific conditions, such as river tides (Fig. 8), ocean tides (Fig. 11) and periodic groundwater extraction patterns (Fig. 7). The identification of harmonic signals in groundwater heads at S_2 and M_2 frequencies provides compelling evidence that the assessed aquifers in the southern VMD respond to external loading. This finding is not limited to the frequency domain but is evident in the time domain as well, providing a scientific framework for the conclusions of Hoang and Steinel (2021) who attribute temporarily rising groundwater heads at IGPVN during the rainy season to loading effects rather than to groundwater recharge by the means of water volume fluxes into the aquifers. However, to evaluate this specific hypothesis, further studies on seasonal surface loading dynamics are necessary.

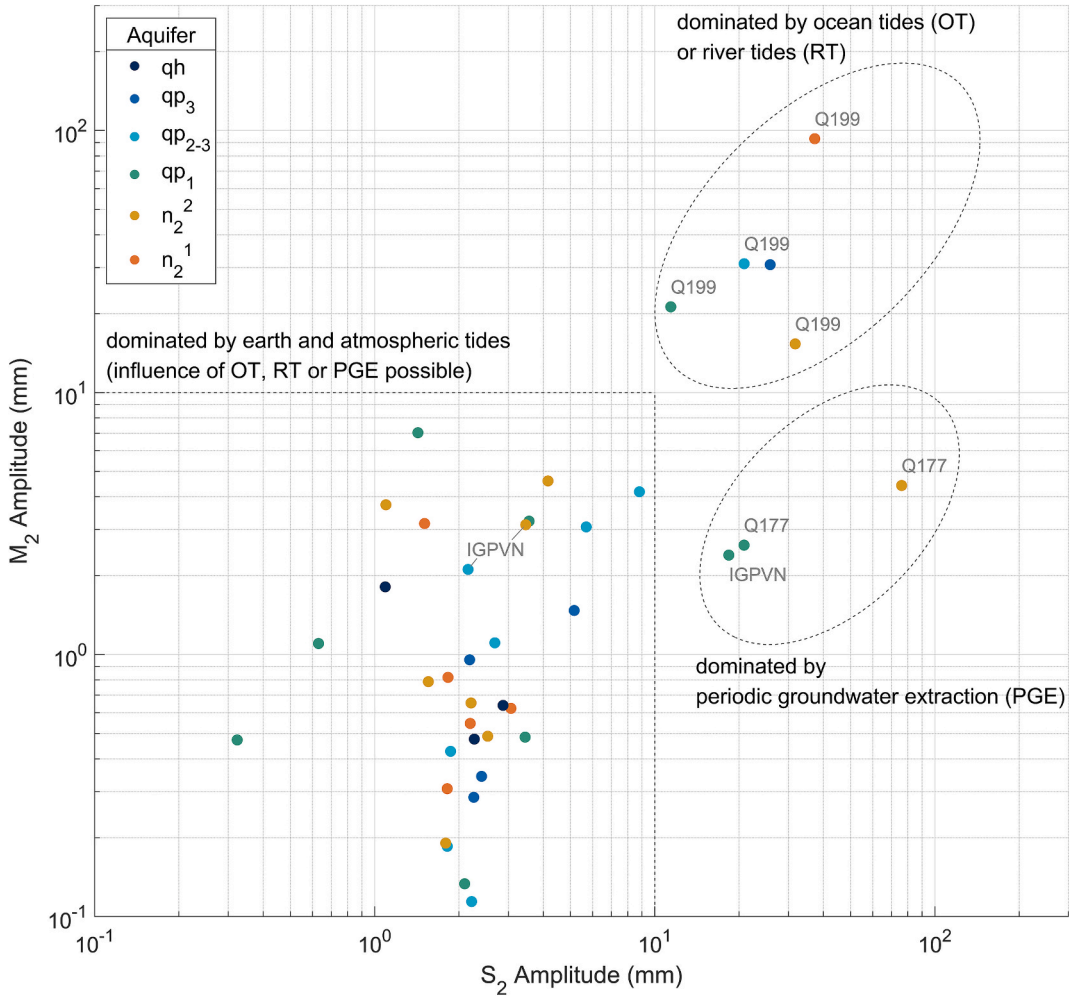

Fig. 6. Preliminary assessment of potential drivers of tidal signals in groundwater heads by a comparison of value and ratio of S_2 and M_2 amplitudes from HALS frequency analyses of 41 observation wells in six different aquifers in the southern VMD.

While the presence of loading signal imprints in groundwater heads is a common feature for confined aquifers (Bredehoeft, 1967), to the authors' best knowledge they have not yet been comprehensively described in the southern VMD. Therefore, the presented study establishes a valuable basis for further research on hydro-geomechanically coupled process dynamics in the study area. By this, the study promotes integrated considerations of hydrogeological and geomechanical problems, of which the observed land subsidence due to groundwater depletion itself is the most prominent example in the study area. In addition, the findings provide a novel perspective on previous studies in the VMD (Duy et al., 2021), which found correlations between ground and surface water levels, without exploring the nature and process dynamics causing the identified correlation.

The southern VMD is a unique study area for PSC-applications in the context of land subsidence due to its complex network of tidally influenced surface water bodies, extensive groundwater extraction and the presence of two distinct ocean tide regimes (Fig. 5). In addition, due to extensive and accelerating land subsidence rates in the low-lying delta, there is an urgent need for hydro-geomechanical subsurface characterization to develop mitigation strategies. If the multiple superposing drivers are carefully disentangled as proposed in this study, the southern VMD and other deltaic groundwater systems bare a high potential to utilize the various tidal forcings for hydro-geomechanical parameter estimations.

5.2. Revelation of multiple influences on groundwater heads

The analyses show that amplitude spectra of groundwater heads can be affected by periodic groundwater extraction patterns (Fig. 7). Demand-oriented operation of municipal water supply wells at scheduled intervals are non-sinusoidal but can leak into FFT-amplitude spectra (Fig. 7f, lines in Fig. 4b-V) at harmonics, i.e., multiples of S_1 and S_2, as well as into HALS-based amplitude characterizations, e.g. at S_2 (dot in Fig. 4b-V). Given that these frequencies are commonly used in PSC, this novel finding highlights the need for careful site-specific analysis prior to PSC applications in densely populated regions with high freshwater demands, such as coastal plains and deltaic lowlands. In the VMD, where up to half a million licensed and unlicensed wells extract groundwater with significant spatiotemporal variability (Danh and Khai, 2015), the potential influence of groundwater extraction patterns on tidal groundwater heads must be carefully considered. Recent applications of time-domain PSC methods have anticipated the effects of groundwater extraction on tidal constituents in groundwater heads (Haehnel et al., 2024). However, to the best of the authors' knowledge, the impact of groundwater extraction patterns on PSC has not yet been demonstrated using actual observational data.

The presented novel approach illustrates that integrating OT_{SE} into PSC enhances the application of PSC in coastal groundwater systems and deltaic lowlands. Here, the consideration of OT_{SE} results in a 10 % increase of volumetric strain from 17.0 nstr to 18.6 nstr and a M_2 phase shift of 3.6° compared to the consideration of only Earth tide strains at

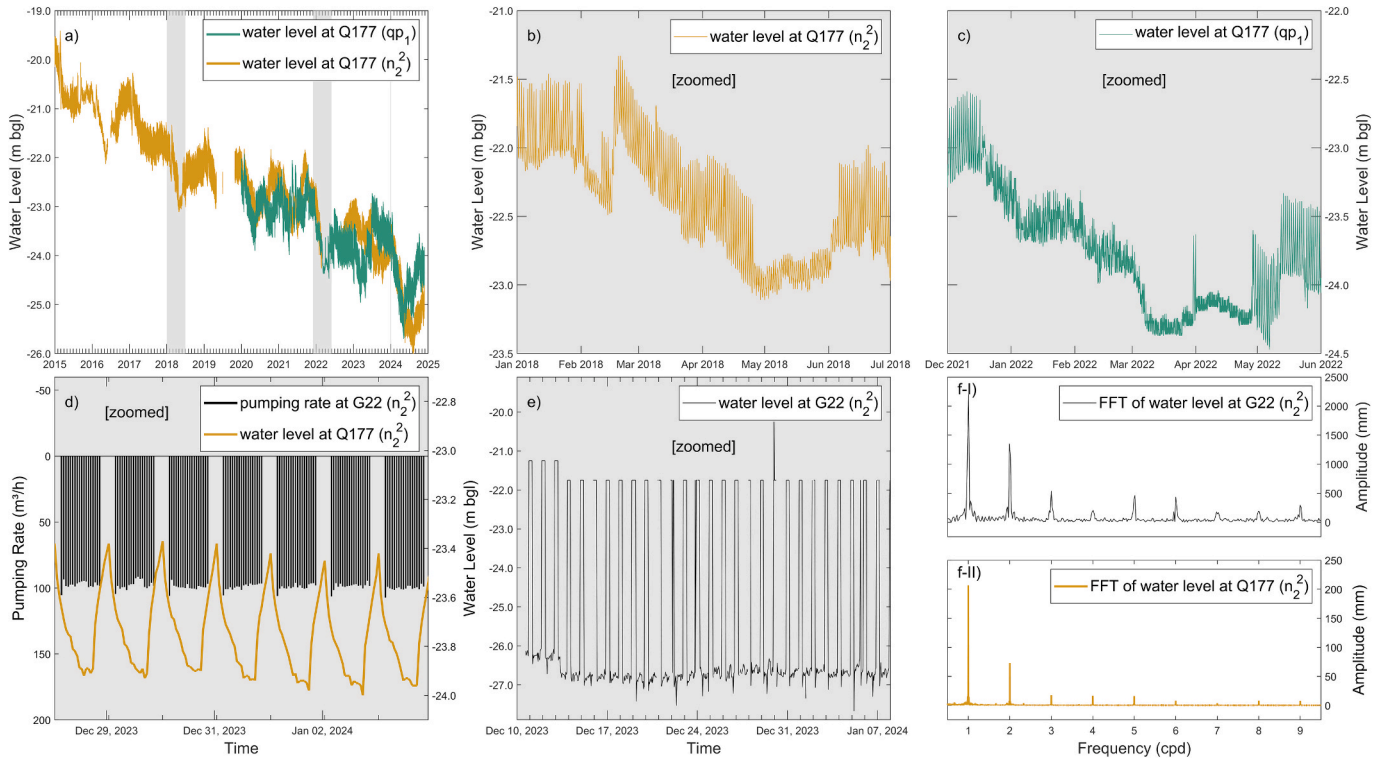

Fig. 7. Groundwater heads in qp_1 and n_2^2 aquifers from 2015 to 2024 at monitoring station Q177 (a), close-up visualization for January to July 2018 in n_2^2 (b) and for December 2021 to May 2022 in qp_1 (c), pumping rates of the water supply well G22 in n_2^2 and groundwater head variations at Q177 in n_2^2 (d), water level dynamics of the pumping well G22 (e) and FFT-amplitude spectra of groundwater heads at G22 (I) and Q177 (II) in n_2^2 aquifer (f).

IGPVN in 15 km distance to the coast (Fig. 11). When OT_{SE} is considered, the phase shift between vented groundwater head records and volumetric strains was determined to be positive in qp_1 aquifer in 2023 (0.9°, Table 2). Given that positive phase shifts are associated with vertical flow in confined systems without borehole skin effects (Valois et al., 2022), this may indicate the presence of aquitard drainage, which is a key process in land subsidence caused by groundwater depletion (Gambolati and Teatini, 2021).

Groundwater pumping for municipal water supply in qp_1 at a distance of 820 m from the observation well could lead to drainage from the adjacent aquitards into the pumped aquifer qp_1 providing a realistic scenario at the investigated study site. The identification of vertical flow using PSC complies with results obtained from a conventional pumping test, characterizing the intermitted aquitard between qp_1 and n_2^2 as leaky at IGPVN (Pechstein et al., 2018).

The study illustrates that careful disentanglement of multiple drivers of tidal signals in groundwater heads is required in regions with multiple tidal forcings. The harmonic forcings of tidally influenced rivers in close vicinity to wells can significantly exceed Earth and atmospheric tidal forcings (Fig. 6), leading to imprints in aquifers at depths exceeding 300 m (Fig. 8). Fig. 8d shows that the groundwater head response at the two major diurnal frequencies K_1 and O_1 is weaker (shifted to the left from the dashed line) compared to responses to the semi-diurnal frequencies M_2 and S_2, which is in line with the known frequency dependency of amplitude damping (Valois et al., 2022). In such settings, where harmonic forcings act on the surface and propagate downwards into the subsurface sediments, a vertically differentiated evaluation of the aquitard hydraulic diffusivity would be possible using an assessment of phase and amplitude difference in the adjacent aquifers (Boldt-Leppin and Hendry, 2003; Larroque et al., 2013).

The aquitard hydraulic diffusivity is equivalent to the consolidation coefficient c_v, a term more commonly used in geomechanical research, describing the delayed compaction response of an aquitard (Gambolati and Teatini, 2021) and is relevant and useful in the context of land subsidence analysis. However, unlike the tidal signals in n_2^1 aquifer (Fig. 4a-VI), the amplitude spectra from the aquifers qp_3, $qp_{2\text{-}3}$, qp_1 and n_2^2 (Fig. 4a-II–a-V) are characterized by a much less precise frequency representation of the river's tidal constituents (Fig. 8a). The cause for the blurred frequency representation (Fig. 4a-II–a-V) needs to be further evaluated before the aquitard hydraulic diffusivity can be assessed using amplitude damping and phase shift. This should include a careful consideration of potential timing errors due to clock drift (Rau et al., 2019).

The novel integration of ocean tide loading on the solid Earth in quantitative PSC parameter estimations enhances the application of such passive methods in near-coastal settings such as deltaic aquifer systems.

5.3. Implications for land subsidence mitigation potential

Given the elastic nature of the tidal forcings at play (Bredehoeft, 1967) it is not possible to quantify inelastic parameters using currently available PSC methods. The differentiation between elastic and inelastic stress regimes as well as the transition between these two end-member conditions is of great importance in land subsidence analyses because (i) unlike elastic deformations inelastic deformations are irreversible (Riley, 1969), and (ii) inelastic deformations can be up to 10–100 times greater than elastic deformation for common aquitard sediments (Riley, 1969; Pavelko, 2004). However, benchmark studies on land subsidence due to groundwater depletion in the VMD (Minderhoud et al., 2017) employ lower ratios between inelastic and elastic compressibility of 5:1 for clay aquitards and 3:1 for sandy aquifers, referring to geotechnical studies in the VMD (Toan and Nu, 2013; Thoang and Giao, 2015). This parameterization indicates that one third of the inelastic aquifer compaction would be reversible, thereby emphasizing the importance of investigating elastic aquifer parameters. This is substantiated by estimations of the overconsolidation ratio *OCR* to approximately 1.6 (Minderhoud et al., 2017) based on a calibrated subsidence model and

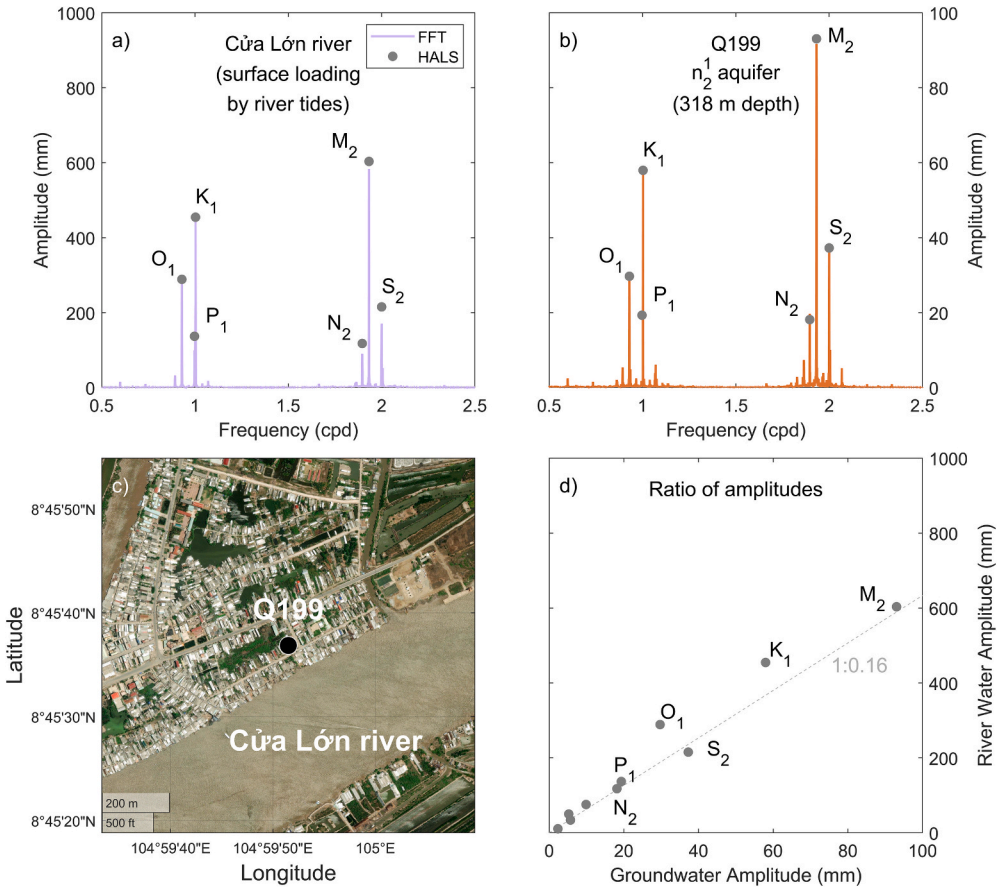

Fig. 8. FFT amplitude spectra (lines) and HALS amplitudes (calculated for the 10 frequencies listed in Table 1, displayed for O_1, K_1, P_1, N_2, M_2 and S_2 frequency as dots) of water levels of the Cửa Lớn river in Nam Can (a) and of groundwater heads in n_2^1 aquifer at monitoring site Q199 (b), satellite image (Esri, 2024) illustrating the location of the groundwater monitoring site and its close distance to the Cửa Lớn river (c), ratio of the HALS amplitudes in groundwater and river water levels of the Cửa Lớn river and n_2^1 aquifer at Q199 (d).

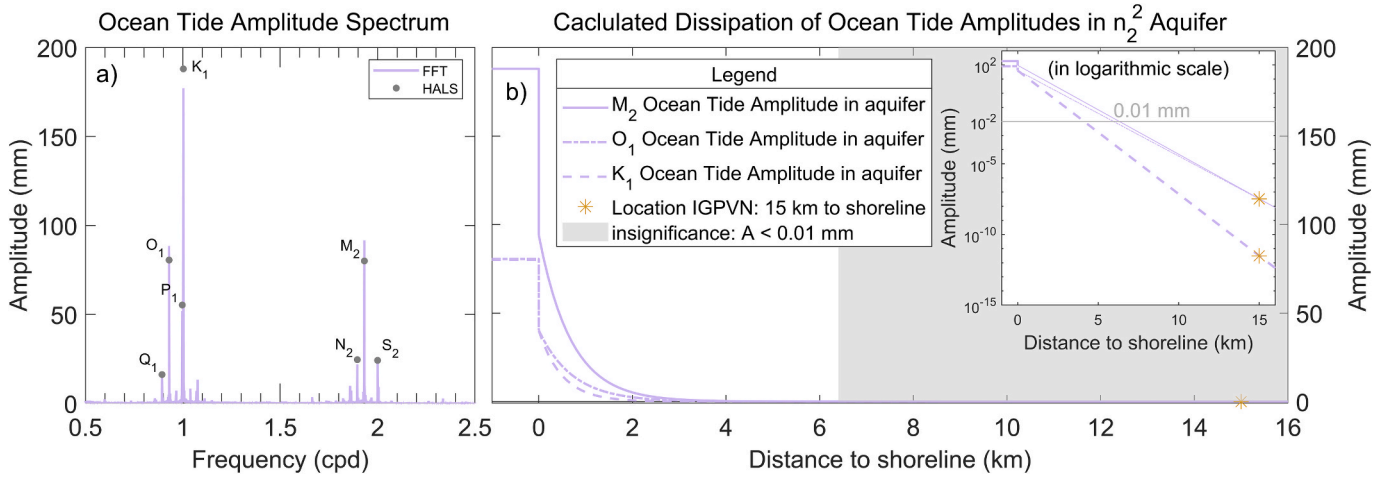

Fig. 9. FFT amplitude spectrum (lines) and HALS amplitudes (calculated for the 10 frequencies listed in Table 1, displayed for Q_1, O_1, K_1, P_1, N_2, M_2 and S_2 frequency as dots) of ocean tides in the Gulf of Thailand, derived from the amplitude spectrum of river water levels at Song Doc (a), calculated amplitude damping of M_2, O_1 and K_1 frequency due to OT_{GW} from the coast towards the inland (b).

the consideration of various geotechnical analyses (Hoang et al., 2016; Thoang and Giao, 2015). Given that $OCR > 1$ is indicative for sediments which have historically experienced stress beyond the current stress, this implies the presence of elastic deformation regimes (Hoffmann et al., 2003).

In the presented study, the elastic specific storage was derived at a selected monitoring site in the southern VMD for $qp_{2\text{-}3}$ and n_2^2 aquifer by two independent PSC methods, i.e., (i) well water level responses to S_2 atmospheric tides ($BE_{S_2}^{AT}$), and (ii) well water level responses to M_2 Earth and ocean tide strains. Both methods deliver consistent results with values between $5.9 \cdot 10^{-6}$ and $8.8 \cdot 10^{-6}$ (m^{-1}) (Table 3). For the n_2^2 aquifer, the S_s estimates from passive methods are verified by

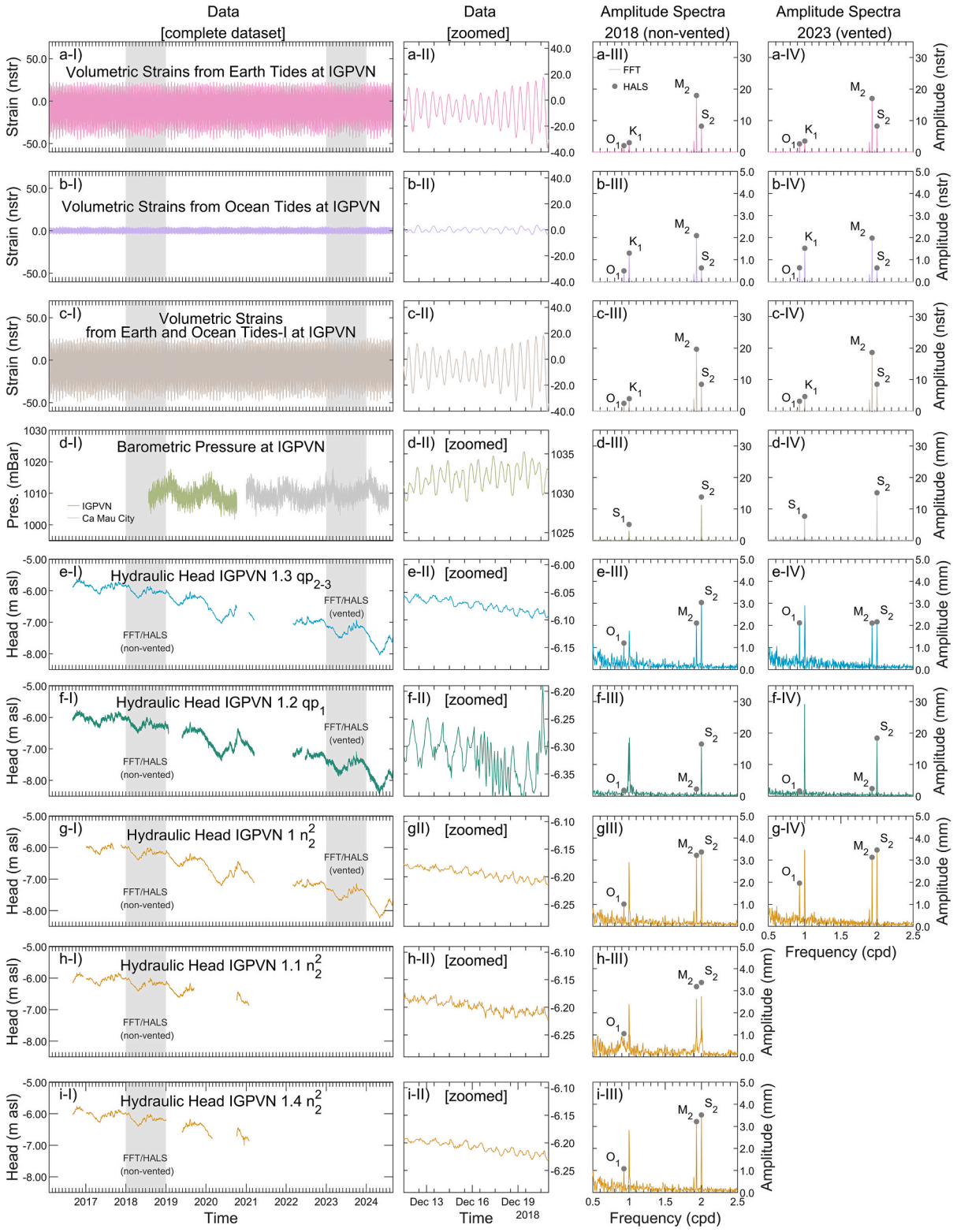

Fig. 10. Employed data (I and II) for the frequency analysis at IGPVN and the resulting FFT amplitude spectrum (lines) and HALS amplitudes (calculated for the 10 frequencies listed in Table 1, displayed for O_1, K_1, S_1, M_2 and S_2 frequency as dots) for 2018 (III) and 2023 (IV), for volumetric Earth tide strains (a) ocean tide strains (b), the sum of Earth and ocean tide strains (c), barometric pressure (d), groundwater heads in the aquifers $qp_{2\text{-}3}$ (e), qp_1 (f) and n_2^2 (g–i).

independently conducted pumping test results of $6.3 \cdot 10^{-6}$ m^{-1} (Pechstein et al., 2018). The derived parameter values are at the lower end of common parameter ranges for aquifers (Domenico and Mifflin, 1965; Rau et al., 2018) and therefore indicate a minimum elastic groundwater storage capacity of the two investigated aquifers. On a regional scale, previous studies derived average parameter values for the storage coefficient S in the n_2^2 aquifer of $1.07 \cdot 10^{-4}$ (–) and an average aquifer thickness of 47.6 m (DWRPIS, 2010; Pechstein et al., 2018). From this, an average specific storage S_s of $2.3 \cdot 10^{-6}$ m^{-1} can be derived, confirming the order of magnitude of the S_s parameter range

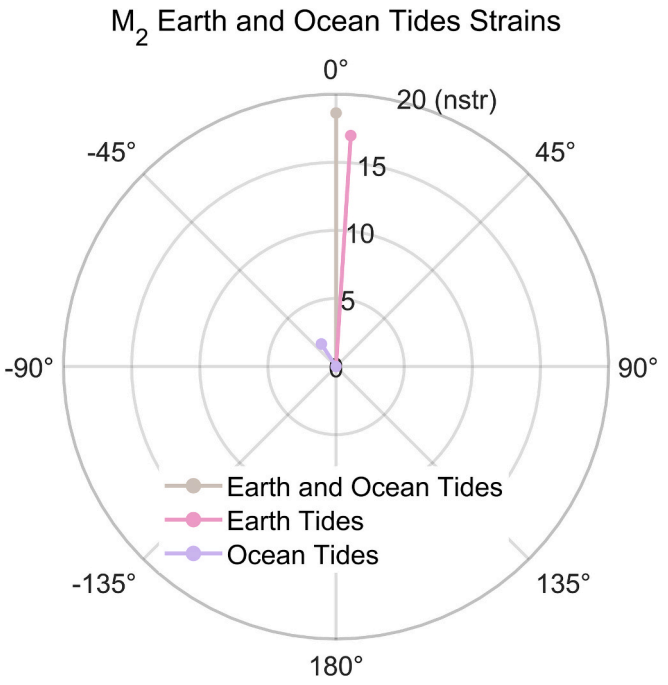

Fig. 11. Polar plot showing M_2 amplitude and phase of volumetric strains due to Earth tides $\widehat{z}_{M_2}^{ET}$ and due to OT_{SE} $\widehat{z}_{M_2}^{OT_{SE}}$ as well as their sum $\widehat{z}_{S_2}^{\{ET+OT_{SE}\}}$ at IGPVN, the phase is referenced to the phase of $\widehat{z}_{S_2}^{\{ET+OT_{SE}\}}$.

between $5.9 \cdot 10^{-6}$ and $7.8 \cdot 10^{-6}$ m^{-1} derived in this study by various passive methods.

The introduction of PSC methods for the estimation of the elastic specific storage is particularly beneficial for the study area, given that the degree of accuracy for S_s-estimates is often below that for transmissivity in pumping tests (Kruseman et al., 1994), particularly in single-well pumping tests. Although the NGMN multi-depth groundwater monitoring sites provide a valuable depth-differentiated dataset in the study area, at most sites each aquifer is only monitored by a single well. In contrast to single-well pumping tests, the deployment of multiple observation wells in one aquifer enhances the reliability of pumping test results (Kruseman et al., 1994), making the parameters derived from pumping test in n_2^2 aquifer at IGPVN a valuable reference for comparison with PSC derived parameters. The good agreement between PSC-based and pumping test-based S_s calculations in n_2^2 at IGPVN demonstrates the usefulness of applying PSC to derive S_s estimations in the southern VMD and other deltaic groundwater bodies.

With the available information of aquifer porosity and thickness, the elastic compaction (and rebound) for $qp_{2\text{-}3}$ and n_2^2 aquifer at IGPVN were estimated with $\alpha = 4.5\text{–}6.4 \cdot 10^{-10}$ Pa^{-1} to 0.18–0.30 mm per meter decline (and recovery) of water level in the confined aquifer. However, observed land subsidence rates are of several mm a^{-1} (Dörr et al., 2024) for a measured groundwater depletion rate of 0.25 m a^{-1} (Hoang and Steinel, 2021). This indicates that the elastic aquifer compaction derived for these two aquifers does not contribute significantly to the observed land subsidence rates. This finding does by no means legitimize a risk-free continuation of groundwater extraction in $qp_{2\text{-}3}$ and n_2^2 aquifer, especially given that a significant part of compaction can be expected to occur in the adjacent aquitards rather than the aquifer (Gambolati and Teatini, 2021).

Governmental circulars and decrees (Circular No. 42/2015/TT-BTNMT, Decree 53/2024/ND-CP, Circular 03/2024/ TT-BTNMT) consider MAR as a potential mitigation measure for land subsidence in the VMD. In general, the injection of water into confined aquifers may prove an efficacious land subsidence mitigation measure in two ways, namely (i) seasonal storage of surplus water resources (Seidl et al., 2024) and (ii) repressurizing of groundwater heads (Gambolati and Teatini, 2021). A seasonal storage of surplus freshwater would reduce the annual net groundwater withdrawal and consequently also the depletion of groundwater heads and associated land subsidence. With large volumes of fresh surface water from the Mekong River and high precipitation rates during the monsoon season, significant freshwater quantities are available in the VMD on an annual basis. However, without sufficient storage capacities in the flat topography, this freshwater cannot be retained for the dry season, leading to substitution sourced from groundwater (Wagner et al., 2012).

Given that truly confined aquifers may only receive surplus water by a deformation of the matrix skeleton or the pore water (Bouwer, 2002), a process inherently contained in the definition of the specific storage S_s (Jacob, 1940), the low estimated specific storage of $<9 \cdot 10^{-6}$ m^{-1} suggests that the considered aquifers are unsuitable for a seasonal freshwater storage based on pressurized water injection.

In addition to the reduction of net annual groundwater withdrawal, MAR can counteract land subsidence by repressurizing targeted confined aquifers (Gambolati and Teatini, 2021) with hydraulic impact zones exceeding the extent of storage zones (Dillon et al., 2009). Based on the estimations of elastic compressibility, the land rebound capability of the two investigated aquifer sediments due to a recovery of groundwater heads is in a range of <3 mm for a 10 m groundwater head increase and therefore insignificant. This emphasizes the urgency to minimize further groundwater depletion to prevent further inelastic land subsidence.

To evaluate the overall rebound capability in the southern VMD, it is essential to characterize shallow aquifer and aquitard sediments. This is particularly important because younger and shallow sediments are generally less consolidated, as indicated by the region's sedimentation history (Zoccarato et al., 2018).

While the presented study focuses on the estimation of elastic aquifer parameters, further research on PSC-based determination of aquitard parameters would be valuable for subsidence-related applications. While recent studies developed analytical solutions to derive the aquitard compressibility from groundwater responses to Earth tides (Valois et al., 2024), the solution's non-uniqueness challenges the estimation of reliable parameter values. Moreover, further investigations that aim to differentiate between elastic and inelastic contributions to land subsidence from groundwater depletion in the southern VMD are required, such as depth-differentiated multi-extensometer compaction monitoring (Dörr et al., 2023).

Given that approximately 25 % of the world's population lives on deltaic lowlands (Tamura et al., 2012) and approximately two billion inhabitants live in areas exposed to potential subsidence (Davydzenka et al., 2024), the presented approach has the potential to be applied in many highly populated coastal plains and deltaic lowlands all around the globe to inform more sustainable groundwater management.

6. Conclusions

The study proves that PSC-methods are valuable tools in the assessment of an aquifer's land subsidence mitigation potential. Imprints of tidal signals in groundwater heads (i.e., as measured using well water levels) carry valuable information about elastic geomechanical subsurface properties and process dynamics and can therefore be used to gain insights of significant relevance for the assessment of land subsidence mitigation potential. The specific storage S_s is a key parameter for an aquifer's land subsidence mitigation potential, as it incorporates the aquifer's elastic deformation characteristics. Therefore, S_s estimates provide relevant information on two key concepts in land subsidence mitigation strategies, (i) an aquifer's land rebound potential and (ii) its capability to temporarily receive and store surplus water resources. Due to the complex interplay of multiple tidal forcings, the application of previously available PSC-based parameter estimation methods for S_s was limited in coastal groundwater and subsiding deltaic aquifer systems.

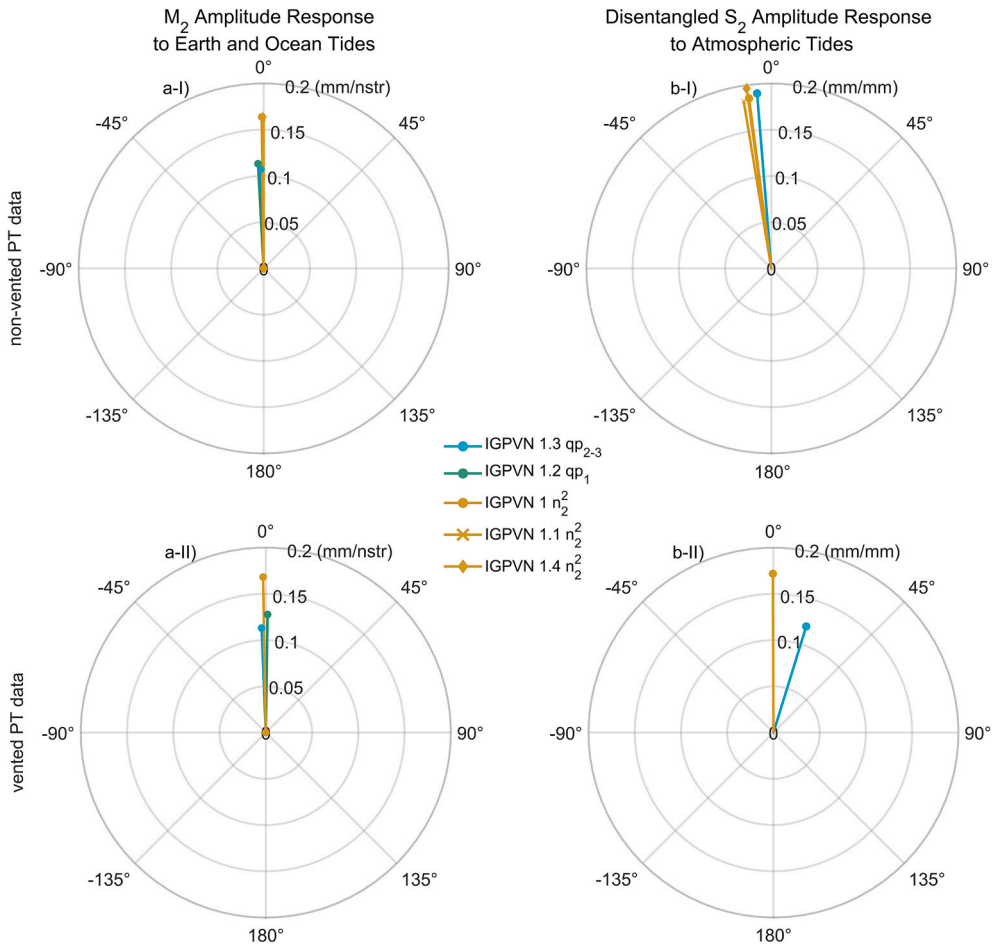

Fig. 12. Polar plots showing amplitude responses to M_2 volumetric strains due to Earth tides and OT_{SE} (a) amplitude response to S_2 atmospheric tides at IGPVN site based on groundwater observation data with non-vented PTs from 2018 (I) and with vented PTs from 2023 (II). It shall be noted that in a-I and b-I, the values for IGPVN 1.1, IGPVN 1.4 and IGPVN 1 are plotted but differ little to insignificantly from each other.

Table 2
Barometric efficiency based on S_2 responses to atmospheric tides BE_{S2}^{AT} as well as M_2 amplitude response A_{M2} and phase shift $\Delta\phi_{M2}$ for wells at the IGPVN site with disentangled Earth and ocean tide influence (calculated values without consideration of ocean tides are additionally displayed in brackets).

	PT	IGPVN 1.3 [qp_{2-3}]	IGPVN 1.2 [qp_1]	IGPVN 1 [n_2^2]	IGPVN 1.1 [n_2^2]	IGPVN 1.4 [n_2^2]
$BE_{S_2}^{AT}$	Non-vented	0.19 (0.19)	–	0.19 (0.18)	0.18 (0.18)	0.20 (0.19)
	vented	0.12 (0.12)	–	0.17 (0.17)		
$\Delta\phi_{M_2}$	Non-vented	−1.7 (−5.3)	−3.1 (−6.7)	−0.8 (−4.4)	−0.1 (−3.7)	−0.3 (−4.0)
	vented	−2.3 (−5.9)	+0.9 (−2.8)	−1.0 (−4.6)		
A_{M_2}	Non-vented	0.11 (0.12)	0.11 (0.12)	0.16 (0.18)	0.16 (0.18)	0.16 (0.18)
	vented	0.11 (0.12)	0.13 (0.14)	0.17 (0.18)		

Table 3
Specific storage at IGPVN derived from PSC and pumping test data.

	BE	θ	S_s (m^{-1}) Earth Tide (Hsieh et al., 1987)	S_s (m^{-1}) Atmospheric Tides Eqs. (9) and (10)	S_s (m^{-1}) Pumping Tests (Pechstein et al., 2018)
IGPVN 1.3 [qp_{2-3}]	0.19	0.33	$8.8 \cdot 10^{-6}$	$7.8 \cdot 10^{-6}$	–
IGPVN 1 [n_2^2]	0.19	0.33	$5.9 \cdot 10^{-6}$	$7.8 \cdot 10^{-6}$	$6.3 \cdot 10^{-6}$

This study demonstrates how to quantitatively disentangle tidal signals in groundwater heads in deltaic aquifer systems, revealing enhanced understanding of subsurface processes and properties in Vietnam's southern Mekong Delta, where loading signals in groundwater heads have not been adequately analyzed before. The findings underscore that further groundwater depletion must be avoided in the Mekong Delta to prevent further irreversible sediment compaction and subsidence. The study emphasizes that PSC-parameter estimations require a careful analysis of local conditions, including groundwater pumping activities, which may corrupt quantitative assessments by leaking into amplitude spectra. Overall, the presented integration of ocean tide loading on the solid Earth enables PSC-parameter estimations in coastal hydrogeological environments.

The presented study is limited to the quantification of elastic aquifer properties. Further research is required to quantify inelastic aquitard compressibility which contributes considerably to the overall observed land subsidence. This could involve the development of new analytical solutions to derive the aquitard compressibility from groundwater responses to cyclic forces.

The methods derived and applied in this study are not limited to the study area of the southern VMD but can be utilized to investigate subsurface hydraulic and geomechanical properties as well as groundwater extraction-related land subsidence in any coastal plain and deltaic lowland. Therefore, this study contributes to inform more sustainable groundwater management in many stressed hydrogeological environments all around the globe.

Overall, this study demonstrates that PSC is a powerful yet underutilized low-cost technique, that may prove particularly valuable for the estimation of hydraulic and geomechanical subsurface properties as well as the evaluation of mitigation strategies in deltas subject to land subsidence due to groundwater depletion.

CRediT authorship contribution statement

Felix Dörr: Writing – original draft, Visualization, Methodology, Investigation, Formal analysis, Data curation, Conceptualization. **Jonas Bauer:** Writing – review & editing, Visualization, Investigation, Formal analysis. **Gabriel C. Rau:** Writing – review & editing, Validation, Methodology, Conceptualization. **Remi Valois:** Writing – review & editing, Software, Conceptualization. **Tran Viet Hoan:** Writing – review & editing, Investigation, Data curation. **Van Cam Pham:** Writing – review & editing. **Le Thi Mai Van:** Writing – review & editing, Project administration, Data curation. **Anke Steinel:** Writing – review & editing, Data curation, Conceptualization. **Franz Nestmann:** Writing – review & editing, Supervision, Resources, Project administration, Funding acquisition, Conceptualization. **Stefan Norra:** Writing – review & editing, Supervision, Resources, Project administration, Funding acquisition.

Declaration of competing interest

The authors declare that they have no known competing financial interests or personal relationships that could have appeared to influence the work reported in this paper.

Acknowledgements

This research was conducted in the frame of the project “ViWaT – Vietnam Water Technologies” funded by the German Federal Ministry of Education and Research (funding reference: 02WCL1474A). Felix Dörr thanks the Hector Fellow Academy for support. We gratefully thank the Vietnamese Ministry of Science and Technology (MOST), the National Center for Water Resources Planning and Investigation (NAWAPI) and the Department of Natural Resources and Environment Ca Mau (DONRE Ca Mau) as well as the Federal Institute for Geosciences and Natural Resources (BGR) who kindly shared the data used in this study. We acknowledge support by the KIT-Publication Fund of the Karlsruhe Institute of Technology, Germany.

Appendix A. Supplementary data

Supplementary data to this article can be found online at https://doi.org/10.1016/j.jhydrol.2025.133844.

Data availability

The well water level data from the sites GW1 and IGPVN (from 2016 to May 2023), as well as the calculated Earth and ocean tide strains for IGPVN and the barometric pressure data used in this study are available at a Zenodo repository: https://doi.org/10.5281/zenodo.14671298. The river water level data, the well water level data from IGPVN after May 2023 as well as the well water level data from the national groundwater monitoring wells are available on request at NAWAPI.

References

Acworth, R.I., Halloran, L.J.S., Rau, G.C., Cuthbert, M.O., Bernardi, T.L., 2016. An objective frequency domain method for quantifying confined aquifer compressible storage using Earth and atmospheric tides. Geophys. Res. Lett. 43, 11671–11678. https://doi.org/10.1002/2016GL071328.

Agnew, D.C., 2007. 3.06 – Earth tides. In: Schubert, G. (Ed.), Treatise on Geophysics. Elsevier, pp. 163–195. https://doi.org/10.1016/B978-044452748-6.00056-0.

Agnew, D.C., 2012. SPOTL: Some Programs for Ocean-Tide Loading, SIO Technical Report. Scripps Institution of Oceanography, UC San Diego, California (last access: 11 November 2024).

Allen, D.R., Mayuga, M.N., 1970. The mechanics of compaction and rebound. International Hydrological Decade, symposium on land subsidence, Tokyo, Japan 17–22 Sept. Wilmington Oil Field, Long Beach, California, USA.

Anderson, H.R., 1978. Hydrogeologic reconnaissance of the Mekong Delta in South Vietnam and Cambodia. Contributions to the hydrology of Asia and Oceania. Geological Survey Water-Supply Paper 1608-R.

Arfken, G., Weber, H., 2005. In: Mathematical Methods for Physicists, 6th ed. Elsevier, Boston, Massachusetts, p. 1182.

Aungsakul, K., Jaroensutasinee, M., Jaroensutasinee, K., 2007. Numerical study of principal tidal constituents in the gulf of Thailand and the Andaman Sea. Walailak J. Sci. Technol. 4 (1), 95–109. https://wjst.wu.ac.th/index.php/wjst/article/view/128.

Baldan, S., Minderhoud, P.S.J., Xotta, R., Zoccarato, C., Teatini, P., 2024. Data-driven 3D modelling of long-term Holocene delta evolution and sediment compaction: the Mekong Delta. Earth Surf. Processes Landf. https://doi.org/10.1002/esp.6046.

Bauer, J., Börsig, N., Pham, V.C., Hoan, T.V., Nguyen, H.T., Norra, S., 2022. Geochemistry and evolution of groundwater resources in the context of salinization and freshening in the southernmost Mekong Delta, Vietnam. J. Hydrol. Reg. Stud. 40. https://doi.org/10.1016/j.ejrh.2022.101010.

Boldt-Leppin, B.E.J., Hendry, M.J., 2003. Application of harmonic analysis of water levels to determine vertical hydraulic conductivities in clay-rich aquitards. Ground Water 41 (4), 514–522. https://doi.org/10.1111/j.1745-6584.2003.tb02385.x.

Bouwer, H., 2002. Artificial recharge of groundwater: hydrogeology and engineering. Hydrgeol. J. 10 (1), 121–142. https://doi.org/10.1007/s10040-001-0182-4.

Bredehoeft, J.D., 1967. Response of well-aquifer systems to Earth tides. J. Geophys. Res. 72 (12), 3075–3087. https://doi.org/10.1029/JZ072i012p03075.

Chen, C.T., Hu, J.T., Lu, C.Y., Lee, J.C., Chan, Y.C., 2007. Thirty-year land elevation change from subsidence to uplift following the termination of groundwater pumping and its geological implications in the Metropolitan Taipei Basin, Northern Taiwan. Eng. Geol. 95, 30–47. https://doi.org/10.1016/j.enggeo.2007.09.001.

Cooper, H.H., 1966. The equation of groundwater flow in fixed and deforming coordinates. J. Geophys. Res. 71 (20), 4785–4790. https://doi.org/10.1029/JZ071i020p04785.

Cui, X., Fang, G., Di, W., 2019. Tidal resonance in the Gulf of Thailand. Ocean Sci. 15 (2), 321–331. https://doi.org/10.5194/os-15-321-2019.

Cutillo, P.A., Bredehoeft, J.D., 2011. Estimating aquifer properties from the water level response to earth tides. Groundwater 49 (4), 600–610. https://doi.org/10.1111/j.1745-6584.2010.00778.x.

Danh, V.T., Khai, H.V., 2015. Household demand and supply for clean groundwater in the Mekong Delta, Vietnam. Renewables 2, 4. https://doi.org/10.1186/s40807-014-0004-7.

Davydzenka, T., Tahmasebi, P., Shokri, N., 2024. Unveiling the global extent of land subsidence: the sinking crisis. Geophys. Res. Lett. 51, e2023GL104497. https://doi.org/10.1029/2023GL104497.

Dillon, P., Pavelic, P., Page, D., Beringen, H., Ward, J., 2009. Managed Aquifer Recharge: An Introduction. ISBN: 978-1-921107-71-9. National Water Commission, Canberra.

Di Giusto, B., Le, T.M.N., Nguyen, T.T.M., Nguyen, T.T.H., Vu, N.U.M., Lavallee, J.P., 2021. Development versus adaptation? Facing climate change in Ca Mau, Vietnam. Atmosphere (Basel) 12. https://doi.org/10.3390/atmos12091160.

Domenico, P.A., Mifflin, M.D., 1965. Water from low-permeability sediments and land subsidence. Water Res. 1 (4), 563–576. https://doi.org/10.1029/WR001i004p00563.

Dörr, N., Schenk, A., Hinz, S., 2021. Analysis of heterogeneous Ps-Insar derived subsidence rates using categorized Gis objects – a case study in the Mekong Delta. Int. Geosci. Remote Sens. Symp. (2021-July), 2655–2658. https://doi.org/10.1109/IGARSS47720.2021.9553297.

Dörr, F., Bauer, J., Tran, H.V., Norra, S., 2023. Vietnams Mekong-Delta – Landsenkung infolge von Grundwasserübernutzung. *Forsch. | WASSERWIRTSCHAFT* 64–68 (in German language). http://doi.org/10.1007/s35147-023-1922-3.

Dörr, N., Schenk, A., Hinz, S., 2024. Land subsidence in the Mekong Delta derived from advanced persistent scatterer interferometry with an infrastructural reference network. IEEE J. Sel. Top. Appl. Earth Obs. Remote Sens. 1–19. https://doi.org/10.1109/JSTARS.2024.3420130.

DWRPIS, 2010. Analysis of the groundwater abstraction status, and assessment of available groundwater resources for water supply, Report 2. Division for Water Resources Planning and Investigation for the south of Vietnam (unpublished).

Erban, L.E., Gorelick, S.M., Zebker, H.A., 2014. Groundwater extraction, land subsidence, and sea-level rise in the Mekong Delta. Vietnam. Environ. Res. Lett. 9. https://doi.org/10.1088/1748-9326/9/8/084010.

EROS, 2017. Global 30 arc-second elevation (GTOPO30). U.S. Geological Survey. [WWW Document]. Earth Resour. Obs. Sci. Cent. https://doi.org/10.5066/F7DF6PQS.

Eslami, S., Hoekstra, P., Nguyen Trung, N., Ahmed Kantoush, S., Van Binh, D., Duc Dung, D., Tran Quang, T., van der Vegt, M., 2019. Tidal amplification and salt intrusion in the Mekong Delta driven by anthropogenic sediment starvation. Sci. Rep. 9, 1–10. https://doi.org/10.1038/s41598-019-55018-9.

Esri, 2024. World Imagery. With assistance of Maxar, Earthstar Geographics, and the GIS User Community, updated on 11/19/2024.
Gambolati, G., Teatini, P., 2021. Land Subsidence and its Mitigation. The Groundwater Project. ISBN: 978-1-77470-001-3.
GSOV, 2024. General Statistics Office of Vietnam. URL (10.2024): https://www.gso.gov.vn/en/homepage/.
Haehnel, P., Rasmussen, T.C., Rau, G.C., 2024. Technical note: removing dynamic sea-level influences from groundwater-level measurements. Hydrol. Earth Syst. Sci. 28 (12), 2767–2784. https://doi.org/10.5194/hess-28-2767-2024.
Herrera-García, G., Ezquerro, P., Tomás, R., Béjar-Pizarro, M., López-Vinielles, J., Rossi, M., et al., 2021. Mapping the global threat of land subsidence. Science 371 (6524), 34–36. https://doi.org/10.1126/science.abb8549.
HGS, 2023. HydroGeoSines, https://github.com/HydroGeoSines/HydroGeoSines (accessed on 9/13/2024).
Hoan, T.V., Richter, K.-G., Börsig, N., Bauer, J., Ha, N.T., Norra, S., 2022. An improved groundwater model framework for aquifer structures of the quaternary-formed sediment body in the southernmost parts of the Mekong Delta, Vietnam. Hydrology 9, 61. https://doi.org/10.3390/hydrology9040061.
Hoang, T.M., van Lap, N., Oanh, T.T.K., Jiro, T., 2016. The influence of delta formation mechanism on geotechnical property sequence of the late Pleistocene-Holocene sediments in the Mekong River Delta. Heliyon 2, e00165. https://doi.org/10.1016/j.heliyon.2016.e00165.
Hoang, T.H., Steinel, A., 2021. Technical Note TN-IV-01. Groundwater level monitoring data at the U Minh well group September 2016 to October 2020. https://www.bgr.bund.de/EN/Themen/Wasser/Projekte/abgeschlossen/TZ/Vietnam/techn_note IV-01_en.pdf?_blob=publicationFile&v=4.
Hoanh, C.T., Phong, N.D., Gowing, J.W., Tuong, T.P., Ngoc, N.V., Hien, N.X., 2009. Hydraulic and water quality modeling: a tool for managing land use conflicts in inland coastal zones. Water Policy 11 (S1), 106–120. https://doi.org/10.2166/wp.2009.107.
Hoffmann, J., Leake, S., Galloway, D., Wilson, A., 2003. MODFLOW-2000 Ground-water model: user guide to the subsidence and aquifersystem compaction (SUB) package. US Geol. Surv. Open-File Rep.
Hsieh, P.A., Bredehoeft, J.D., Farr, J.M., 1987. Determination of aquifer transmissivity from Earth tide analysis. Water Res. 23 (10), 1824–1832. https://doi.org/10.1029/WR023i010p01824.
Jacob, C.E., 1940. On the flow of water in an elastic artesian aquifer. Eos Trans. AGU 21 (2), 574–586. https://doi.org/10.1029/TR021i002p00574.
Jacob, C.E., 1950. Flow of groundwater. Eng. Hydraul. 321–386.
Klönne, F.W., 1880. Die periodischen Schwankungen des Wasserspiegels in den inundieten Kohlenschachten von Dux in der Periode von 8 April bis 15 September 1879. Sitzungsberichte Kaiserliche Akademie Der Wissenschaften.
Kondolf, G.M., Schmitt, R.J.P., Carling, P.A., Goichot, M., Keskinen, M., Arias, M.E., Bizzi, S., Castelletti, A., Cochrane, T.A., Darby, S.E., Kummu, M., Minderhoud, P.S.J., Nguyen, D., Nguyen, H.T., Nguyen, N.T., Oeurng, C., Opperman, J., Rubin, Z., San, D.C., Schmeier, S., Wild, T., 2022. Save the Mekong Delta from drowning. Science (80-.) 376, 583–585. https://doi.org/10.1126/science.abm5176.
Kruseman, G.P., De Ridder, N.A., Verweij, J.M., 1994. Analysis and Evaluation of Pumping Test Data, (Completely Revised). International Institute for Land Reclamation and Improvement, Netherlands.
Larroque, F., Cabaret, O., Atteia, O., Dupuy, A., Franceschi, M., 2013. Vertical heterogeneities of hydraulic aquitard parameters: preliminary results from laboratory and in situ monitoring. Hydrol. Sci. J. 58 (4), 912–929. https://doi.org/10.1080/02626667.2013.783215.
Duy, N.L., Nguyen, T.V.K., Nguyen, D.V., Tran, A.T., Nguyen, H.T., Heidbüchel, I., 2021. Groundwater dynamics in the Vietnamese Mekong Delta: trends, memory effects, and response times. J. Hydrol. Reg. Stud. 33, 100746. https://doi.org/10.1016/j.ejrh.2020.100746.
MATLAB, 2023. MATLAB. Version 23.2.0. (R2023b). The MathWorks Inc., Natick, Massachusetts. Available online at https://www.mathworks.com.
McMillan, T.C., Rau, G.C., Timms, W.A., Andersen, M.S., 2019. Utilizing the impact of earth and atmospheric tides on groundwater systems: a review reveals the future potential. Rev. Geophys. 57, 281–315. https://doi.org/10.1029/2018RG000630.
Merritt, M.L., 2004. Estimating Hydraulic Properties of the Floridan Aquifer System by Analysis of Earth-Tide, Ocean-Tide, and Barometric Effects, Collier and Hendry Counties (No. 3). US Department of the Interior, US Geological Survey.
Minderhoud, P.S.J., Erkens, G., Pham, V.H., Bui, V.T., Erban, L., Kooi, H., Stouthamer, E., 2017. Impacts of 25 years of groundwater extraction on subsidence in the Mekong delta, Vietnam. Environ. Res. Lett. 12 (6), 64006. https://doi.org/10.1088/1748-9326/aa7146.
Minderhoud, P.S.J., Coumou, L., Erkens, G., Middelkoop, H., Stouthamer, E., 2019. Mekong delta much lower than previously assumed in sea-level rise impact assessments. Nat. Commun. 10, 1–13. https://doi.org/10.1038/s41467-019-11602-1.
Minderhoud, P.S.J., Middelkoop, H., Erkens, G., Stouthamer, E., 2020. Groundwater extraction may drown mega-delta: projections of extraction-induced subsidence and elevation of the Mekong delta for the 21st century. Environ. Res. Commun. 2, 011005. https://doi.org/10.1088/2515-7620/ab5e21.
Motagh, M., Walter, T.R., Sharifi, M.A., Fielding, E., Schenk, A., Anderssohn, J., Zschau, J., 2008. Land subsidence in Iran caused by widespread water reservoir overexploitation. Geophys. Res. Lett. 35 (16), L16403. https://doi.org/10.1029/2008GL033814.
NAWAPI, 2018. Report Phase I, Upgrade and Build Groundwater Monitoring Network in the Mekong Delta in the Context of Climate Change. NAWAPI, Hanoi, Vietnam (unpublished).
Neussner, O., 2019. Trouble Underground. Land Subsidence in the Mekong Delta. Deutsche Gesellschaft für Internationale Zusammenarbeit (GIZ).
Nguyen, N.T., 2020. Evolution of water levels at coastal hydrological stations of the Mekong Delta. In: Nguyen, K.D., Guillou, S., Gourbesville, P., Thiebot, J. (Eds.), Estuaries and Coastal Zones in times of Global Change. Springer Water, Singapore, pp. 831–843. https://doi.org/10.1007/978-981-15-2081-5_48.
Nguyen, T.H.O., Tran, T.T.K., Nguyen, C.T.H., 2019. Shrimp yield in relation to the ecological parameters of an organic shrimp model in the Mekong Delta of Vietnam: a case study. Asian Fish. Sci. 32, 154–161. https://doi.org/10.33997/j.afs.2019.32.4.003.
Patton, A.M., Rau, G.C., Cleall, P.J., Cuthbert, M.O., 2021. Hydro-geomechanical characterisation of a coastal urban aquifer using multiscalar time and frequency domain groundwater-level responses. Hydrogeol. J. 29 (8), 2751–2771. https://doi.org/10.1007/s10040-021-02400-5.
Pavelko, M.T., 2004. Estimates of hydraulic properties from a onedimensional numerical model of vertical aquifer-system deformation, Lorenzi site, Las Vegas, Nevada. US Geol. Surv. Water Resour. Rep. 2003–4083. https://doi.org/10.3133/wri034083.
Pechstein, A., Hoang, T.H., Orilski J., Le H.N., Le V.M., 2018. Detailed Investigations on the Hydrogeological Situation in Ca Mau Province, Mekong Delta. Technical Report No III-5. BGR. Ho Chi Minh City. https://www.bgr.bund.de/EN/Themen/Wasser/Projekte/abgeschlossen/TZ/Vietnam/techn_repIII-5_en.pdf;jsessionid=EDD60573B567BB1E9C2B0B5B61478AE1.1_cid331?_blob=publicationFile&v=2.
Pham, V.C., Bauer, J., Börsig, N., Ho, J., Vu, L., Tran, H., Dörr, F., Norra, S., 2023. Groundwater use habits and environmental awareness in Ca Mau Province, Vietnam : implications for sustainable water resource management. Environ. Challenges 13, 100742. https://doi.org/10.1016/j.envc.2023.100742.
Pham, H.V., Van Geer, F.C., Tran, V.B., Dubelaar, W., Oude Essink, G.H.P., 2019. Paleo-hydrogeological reconstruction of the fresh-saline groundwater distribution in the Vietnamese Mekong Delta since the late Pleistocene. J. Hydrol. Reg. Stud. 23, 100594. https://doi.org/10.1016/j.ejrh.2019.100594.
Poland, J.F., Davis, G.H., 1969. Land subsidence due to withdrawal of fluids. GSA Rev. Eng. Geol. 2, 187–269. https://doi.org/10.1130/REG2-p187.
Rau, G.C., Acworth, R.I., Halloran, L.J.S., Timms, W.A., Cuthbert, M.O., 2018. Quantifying compressible groundwater storage by combining cross-hole seismic surveys and head response to atmospheric tides. J. Geophys. Res.: Earth Surf. 123 (8), 1910–1930. https://doi.org/10.1029/2018JF004660.
Rau, G.C., Post, V.E.A., Shanafield, M., Krekeler, T., Banks, E.W., Blum, P., 2019. Error in hydraulic head and gradient time-series measurements: a quantitative appraisal. Hydrol. Earth Syst. Sci. 23 (9), 3603–3629. https://doi.org/10.5194/hess-23-3603-2019.
Rau, G.C., Cuthbert, M.O., Acworth, R.I., Blum, P., 2020. Technical note: disentangling the groundwater response to Earth and atmospheric tides to improve subsurface characterisation. Hydrol. Earth Syst. Sci. 24, 6033–6046. https://doi.org/10.5194/hess-24-6033-2020.
Rau, G.C., McMillan, T.C., Andersen, M.S., Timms, W.A., 2022. In situ estimation of subsurface hydro-geomechanical properties using the groundwater response to semi-diurnal Earth and atmospheric tides. Hydrol. Earth Syst. Sci. 26 (16), 4301–4321. https://doi.org/10.5194/hess-26-4301-2022.
Rau, G.C., Eulenfeld T., Howe D., Rietbroek R., Gosselin J.S., Staniewicz S., 2022b. hydrogeoscience/pygtide: PyGTide v0.7.1, Zenodo [code].
Ray, R.D., Ponte, R.M., 2003. Barometric tides from ECMWF operational analyses. Ann. Geophys. 21 (8), 1897–1910. https://doi.org/10.5194/angeo-21-1897-2003.
Riley, F.S., 1969. Analysis of borehole extensometer data from central California. Int. Assoc. Sci. Hydrol. Publ. 89, 423–431.
Roeloffs, E.A., Burford, S.S., Riley, F.S., Records, A.W., 1989. Hydrologic effects on water level changes associated with episodic fault creep near Parkfield, California. J. Geophys. Res. 94 (B9), 12387. https://doi.org/10.1029/jb094ib09p12387.
Rojstaczer, S., 1988. Determination of fluid flow properties from the response of water levels in wells to atmospheric loading. Water Resour. Res. 24 (11), 1927–1938. https://doi.org/10.1029/wr024i011p01927.
Schweizer, D., Ried, V., Rau, G.C., Tuck, J.E., Stoica, P., 2021. Comparing methods and defining practical requirements for extracting harmonic tidal components from groundwater level measurements. Math. Geosci. 53, 1147–1169. https://doi.org/10.1007/s11004-020-09915-9.
Seidl, C., Page, D., Wheeler, S.A., 2024. Using managed aquifer recharge to address land subsidence: insights from a global literature review. Water Secur. 23, 100184. https://doi.org/10.1016/j.wasec.2024.100184.
Siripong, A., 1985. The Characteristics of the Tides in the Gulf of Thailand. Report. Marine Science Department, Chulalongkorn University, Bangkok.
Sreng, S.L., Sugiyama, H., Kusaka, T., Saitoh, M., 2011. Upheaval phenomenon in clay ground induced by rising groundwater level. Poromechanics 4, 196–203.
Sun, H., Grandstaff, D., Shagam, R., 1999. Land subsidence due to groundwater withdrawal: potential damage of subsidence and sea level rise in southern New Jersey, USA. Environ. Geol. 37 (4), 290–296. https://doi.org/10.1007/s002540050386.
Syvitski, J.P.M., Kettner, A.J., Overeem, I., Hutton, E.W.H., Hannon, M.T., Brakenridge, G.R., et al., 2009. Sinking deltas due to human activities. Nat. Geosci. 2 (10), 681–686. https://doi.org/10.1038/ngeo629.
Tamura, T., Saito, Y., Nguyen, V.L., Ta, T.O., Bateman, M.D., Matsumoto, D., Yamashita, S., 2012. Origin and evolution of interdistributary delta plains; insights from Mekong River delta. Geology 40 (4), 303–306. https://doi.org/10.1130/G32717.1.
Thoang, T.T., Giao, P.H., 2015. Subsurface characterization and prediction of land subsidence for HCM City, Vietnam. Eng. Geol. 199, 107–124. https://doi.org/10.1016/j.enggeo.2015.10.009.

Thong, M.T., Thanh, X., Huyen, V.N., Trung, L.D., Cuong, L.P., Van Hung, L., Hung, C.C., Thi, T., Diep, N., Marcille, J., 2010. Expansion of shrimp farming in Ca Mau, Vietnam Ha Thi Phuong Tien, Nguyen Thu Huong. In: Cook, J.A., Cylke, O., Larson, D.F., Nash, J.D., Stedman-Edwards, P. (Eds.), Vulnerable Places, Vulnerable People Trade Liberalization. Rural Poverty and the Environment, pp. 126–144. https://doi.org/10.4337/9781849805193.00015.

Toan, D.M., Nu, N.T., 2013. Studying on the engineering geological characteristics of Middle-Upper Holocene formation (in Vietnamese, English Summary) Tap chi GIA CHAT, loat A so 333 47–56.

Turnadge, C., Crosbie, R.S., Barron, O., Rau, G.C., 2019. Comparing methods of barometric efficiency characterization for specific storage estimation. Groundwater 57 (6), 844–859. https://doi.org/10.1111/gwat.12923.

Valois, R., Rau, G.C., Vouillamoz, J.M., Derode, B., 2022. Estimating hydraulic properties of the shallow subsurface using the groundwater response to Earth and atmospheric tides: a comparison with pumping tests. Water Resour. Res. 58, e2021WR031666. https://doi.org/10.1029/2021WR031666.

Valois, R., Rivière, A., Vouillamoz, J.-M., Rau, G.C., 2024. Technical note: analytical solution for well water response to Earth tides in leaky aquifers with storage and compressibility in the aquitard. Hydrol. Earth Syst. Sci. 28 (4), 1041–1054. https://doi.org/10.5194/hess-28-1041-2024.

Van, P.D.T., Yarina, L., Nguyen, H.Q., Downes, N.K., 2023. Progress toward resilient and sustainable water management in the Vietnamese Mekong Delta. Wires Water 10 (6), e1670. https://doi.org/10.1002/wat2.1670.

Van der Kamp, G., 1972. Tidal fluctuations in a confined aquifer extending under the sea. In: 24th International Geological Congress, Section 11, pp. 101–106. Montreal, Que., Canada.

Van der Kamp, G., Gale, J.E., 1983. Theory of earth tide and barometric effects in porous formations with compressible grains. Water Resour Res 19 (2), 538–544. ISSN 19447973.

Veatch, A.C., 1906. Fluctuations of the Water Level in Wells, with Special Reference to Long Island, New York. Water Supply and Irrigation Paper No. 155. United States Geological Survey, Government Printing Office, Washington, DC.

Wagner, F., Tran, V.B., Renaud, F.G., 2012. Chapter 7, Groundwater resources in the Mekong Delta: availability. In: Renaud Fabrice, K.C.G. (Ed.), The Mekong Delta System – Interdisciplinary Analysis of a River Delta, first ed. Springer, Dordrecht, pp. 201–220. https://doi.org/10.1007/978-94-007-3962-87.

Wenzel, H.-G., 1996. The nanoGal software: Earth tide data processing package: ETERNA 3.3. Bulletin D'informations Des Marées Terrestres 124, 9425–9439.

Xue, L., Brodsky, E.E., Erskine, J., Fulton, P.M., Carter, R., 2016. A permeability and compliance contrast measured hydrogeologically on the San Andreas Fault. Geochem. Geophys. Geosyst. 17 (3), 858–871. https://doi.org/10.1002/2015gc006167.

Zhang, Y., Wu, J., Xue, Y., Wang, Z., Yao, Y., Yan, X., Wang, H., 2015. Land subsidence and uplift due to long-term groundwater extraction and artificial recharge in Shanghai, China. Hydrogeol. J. 23 (8), 1851–1866. https://doi.org/10.1007/s10040-015-1302-x.

Zoccarato, C., Minderhoud, P.S.J., Teatini, P., 2018. The role of sedimentation and natural compaction in a prograding delta: insights from the mega Mekong delta, Vietnam. Sci. Rep. 8, 11437. https://doi.org/10.1038/s41598-018-29734-7.